Electronic Supplementary Material (ESI) for Dalton Transactions.

Electronic Supplementary Information for the Publication

Entitled

Coordination, Reactivity, and Structural Properties of Electron-Rich Ethoxy- and Dimethylamino-Substituted 1,3-Diketiminate Ligands and Their Complexes

Michael A. Land,[a] Bright Huo,[a] Katherine N. Robertson,[a] Kai E. O. Ylijoki,[a] Peter T. K. Lee,[a] Jetsuda Areephong,[a] Dragoslav Vidović[b] and Jason A. C. Clyburne*[a]

[a] *The Atlantic Centre for Green Chemistry, Department of Chemistry, Saint Mary's University, Halifax, Nova Scotia, B3H 3C3, Canada;* [b] *School of Chemistry, Monash University, Melbourne, Victoria 3800, Australia..*

*Corresponding Author. E-mail: Jason.clyburne@smu.ca, Tel: 01 902 420-5827

Summary of Compounds

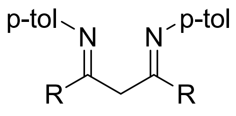

5, R = OEt
6, R = NMe_2

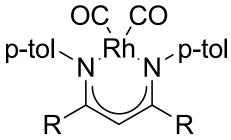

11, R = OEt
12, R = NMe_2

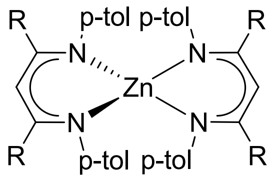

15, R = OEt
16, R = NMe_2

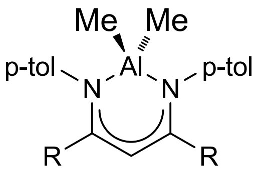

17, R = OEt
18, R = NMe_2

Table of Contents

Deuterium Exchange Study

Ligand precursors **5** and **6** (0.05 mmol) were separately dissolved in of mixture consisting of; 2 mL of D_2O, 1 mL of 1,4-dioxane, and 60 μL (8 mol %) of 0.05 M KOH solution in D_2O. The solution was stirred in a sealed 5 mL vial at 50 °C for 18 hours, resulting in a pale yellow suspension. The supernatant was removed *via* vacuum filtration and an off-white powder was isolated. Reactions conditions/progress were not modified/monitored, therefore, the same results may be obtained in less time, or at lower temperatures. **$D_2C[C(OC_2H_5)(N\textit{p}\text{-}CH_3C_6H_4)]_2$ (5·D_2):** ^{1}H (300 MHz, C_6D_6, ppm): δ 1.15 (t, 6H, $^3J_{HH}$ = 7.1 Hz, $OCH_2C\underline{H}_3$), 2.14 (s, 6H, *p*-$C\underline{H}_3$), 4.25 (q, 4H, J_{HH} = 7.1 Hz, $OC\underline{H}_2CH_3$), 6.67 (d, 4H, $^3J_{HH}$ = 8.0 Hz, *o*-$C\underline{H}$), 6.97 (d, 4H, *m*-$C\underline{H}$). **$D_2C[C(N\{CH_3\}_2)(N\textit{p}\text{-}CH_3C_6H_4)]_2$ (6·D_2):** ^{1}H (300 MHz, C_6D_6, ppm): δ 2.20 (s, 6H, *p*-$C\underline{H}_3$), 2.70 (s, 12H, $NC\underline{H}_3$), 6.65 (d, 4H, *o*-$C\underline{H}$), 7.02 (d, 4H, *m*-$C\underline{H}$).

X-Ray Crystallography

All images presented within this section were prepared using Mercury version 3.6 and all thermal ellipsoids are drawn at the 50 % probability level.

Table S1: Crystal data and structure refinement details

Identification code	**5**	**6**	**11**	**12**	**15**	**16**	**17**	**18**
Empirical formula	$C_{21}H_{26}N_2O_2$	$C_{21}H_{28}N_4$	$C_{23}H_{25}N_2O_4Rh$	$C_{23}H_{27}N_4O_2Rh$	$C_{42}H_{50}N_4O_4Zn$	$C_{42}H_{54}N_8Zn$	$C_{23}H_{33}AlN_4$	$C_{23}H_{31}AlN_2O_2$
Formula weight	338.44	336.47	496.36	494.39	740.23	736.30	392.51	394.48
Crystal system	Triclinic	Monoclinic	Triclinic	Orthorhombic	Triclinic	Monoclinic	Monoclinic	Monoclinic
Space group	*P*-1	$P2_1/c$	*P*-1	*Pbca*	*P*-1	*C2/c*	$P2_1/n$	$P2_1/c$
Unit cell dimensions (Å and °)	*a* = 7.8526(14)	23.757(4)	9.7606(9)	15.376(5)	11.4917(2)	17.462(2)	17.128(2)	8.6122(12)
	b = 10.4721(18)	7.5454(11)	10.5377(10)	14.622(5)	11.5000(2)	10.8487(14)	8.9959(10)	21.655(3)
	c = 13.253(2)	21.366(3)	11.5641(11)	20.208(6)	17.1243(3)	21.572(3)	17.166(2)	12.1405(1)
	α = 112.609(2)	90	96.6850(10)	90	72.7160(10)	90	90	90
	β = 93.693(2)	93.621(2)	103.8860(10)	90	77.5890(10)	105.3770(10)	118.633(2)	90.039(2)
	γ = 101.864(2)	90	98.2180(10)	90	64.8750(10)	90	90 90	
Volume (Å^3)	972.1(3)	3822.4(10)	1128.65(18)	4543(2)	1946.07(6)	3940.4(9)	2321.5(5)	2264.2(5)
Z	2	8	2	8	2	4	4	4
Density (calculated, Mg/m^3)	1.156	1.169	1.461	1.446	1.263	1.241	1.123	1.157
Absorption coefficient (mm^{-1})	0.074	0.071	0.787	0.777	0.677	0.663	0.102	0.109
F(000)	364	1456	508	2032	784	1568	848	848
Crystal size (mm^3)	0.160x0.120x0.080	0.300x0.200x0.080	0.200x0.100x0.080	0.225x0.110x0.090	0.240x0.140x0.120	0.200x0.120x0.100	0.280x0.230x0.180	0.200x0.180x0.120
Theta range of data (°)	2.142 to 28.940	2.143 to 28.925	2.184 to 28.918	2.170 to 28.915	1.252 to 28.829	2.233 to 28.934	2.328 to 29.157	1.881 to 27.384
Index ranges	-10<=h<=10	-31<=h<=32	-13<=h<=13	-20<=h<=20	-15<=h<=15	-22<=h<=23	-22<=h<=22	-11<=h<=11
	-13<=k<=14	-9<=k<=10	-14<=k<=14	-18<=k<=19	-15<=k<=15	-14<=k<=14	-10<=k<=11	-27<=k<=27
	-17<=l<=17	-28<=l<=28	-15<=l<=15	-26<=l<=27	-23<=l<=22	-29<=l<=27	-22<=l<=12	-15<=l<=15
Reflections collected	11909	44914	13739	52413	34049	23441	27970	25718
Independent reflections	4707	9521	5422	5799	9316	4936	5164	5078
R(int)	0.0219	0.0440	0.0160	0.0434	0.0400	0.0519	0.0618	0.0564
Completeness to 25.242° (%)	99.7	99.9	99.7	100.0	99.8	100.0	94.7	100.0
Max. / min. transmission	0.7458 / 0.7012	0.7458 / 0.7000	0.7458 / 0.6868	0.7458 / 0.6850	0.7458 / 0.6990	0.7458 / 0.6871	0.7458 / 0.5707	0.7455 / 0.6581
Data / restraints / parameters	4707 / 0 / 229	9521 / 0 / 460	5422 / 0 / 275	5799 / 0 / 277	9316 / 0 / 467	4936 / 0 / 237	5164 / 0 / 261	5078 / 0 / 259
Goodness-of-fit on F^2	1.038	1.022	1.032	1.014	1.041	1.019	1.042	1.033
Final R indices [I>2sigma(I)]	R1 = 0.0417	0.0460	0.0205	0.0252	0.0376	0.0350	0.0424	0.0415
	wR2 = 0.0966	0.1043	0.0497	0.0549	0.0887	0.0791	0.1083	0.0866
R indices (all data)	R1 = 0.0589	0.0748	0.0234	0.0399	0.0539	0.0478	0.0518	0.0589
	wR2 = 0.1058	0.1182	0.0513	0.0606	0.0961	0.0850	0.1160	0.0931
Largest diff. peak and hole (e.Å^{-3})	0.235 / -0.201	0.296 / -0.219	0.345 / -0.371	0.425 / -0.333	0.461 / -0.410	0.368 / -0.329	0.334 / -0.297	0.205/-0.227

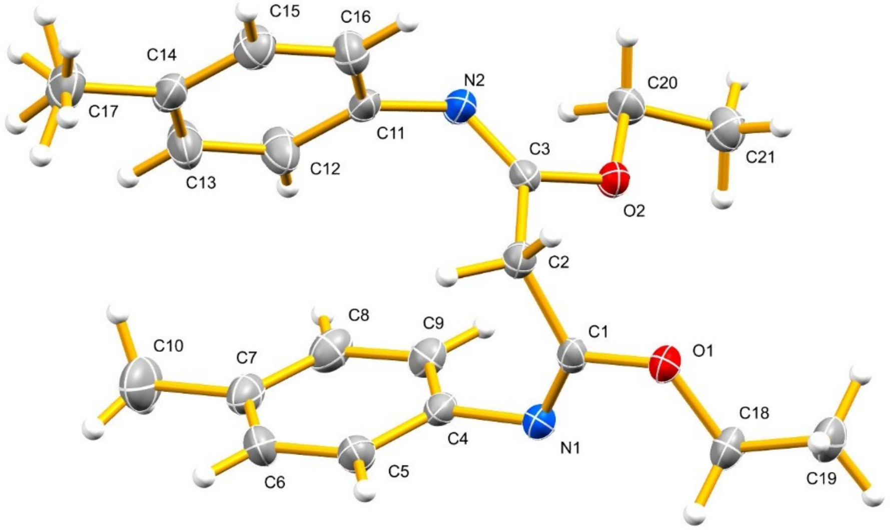

Figure S1: Solid state structure of **5** with all heavy atoms labelled.

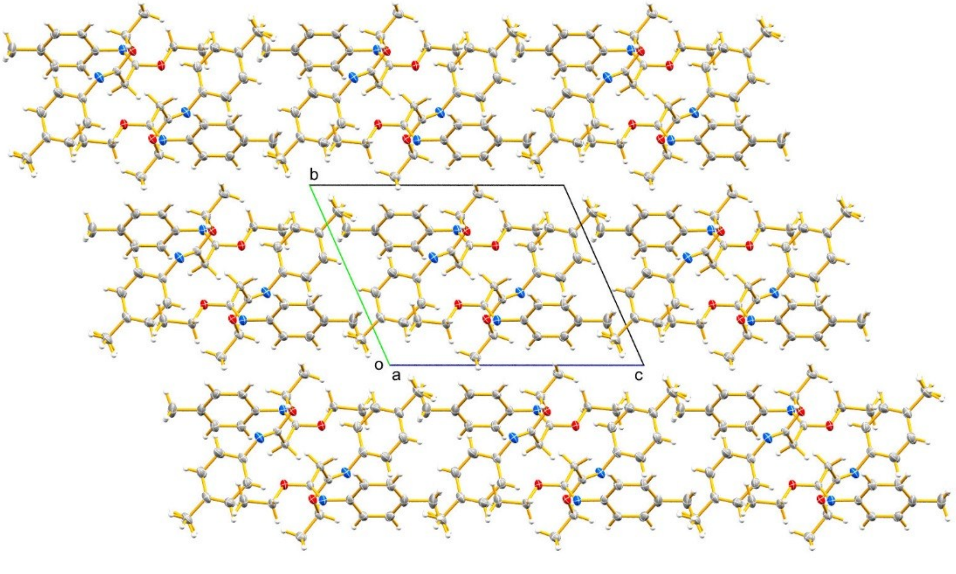

Figure S2: Solid state packing diagram of **5**, viewed down the *X*-axis.

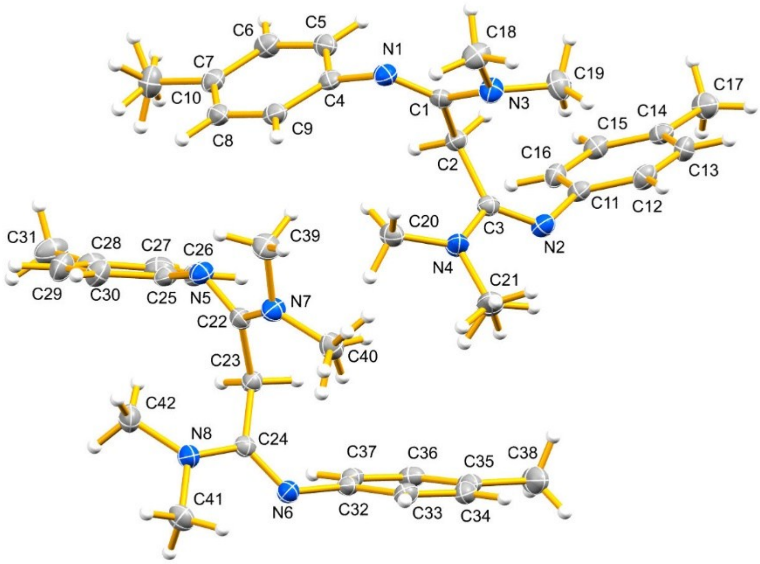

Figure S3: Solid state structure of **6** with all heavy atoms labelled.

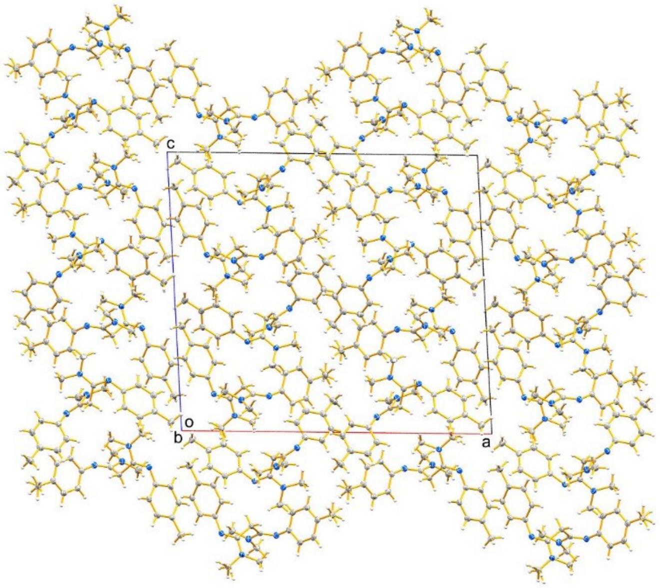

Figure S4: Solid state packing diagram of **6**, viewed down the *Y*-axis.

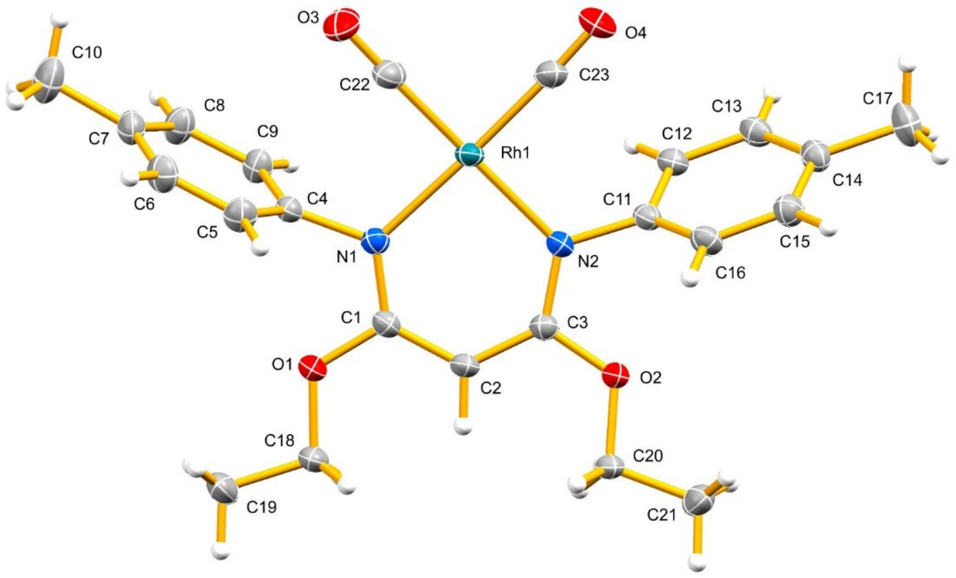

Figure S5: Solid state structure of **11** with all heavy atoms labelled.

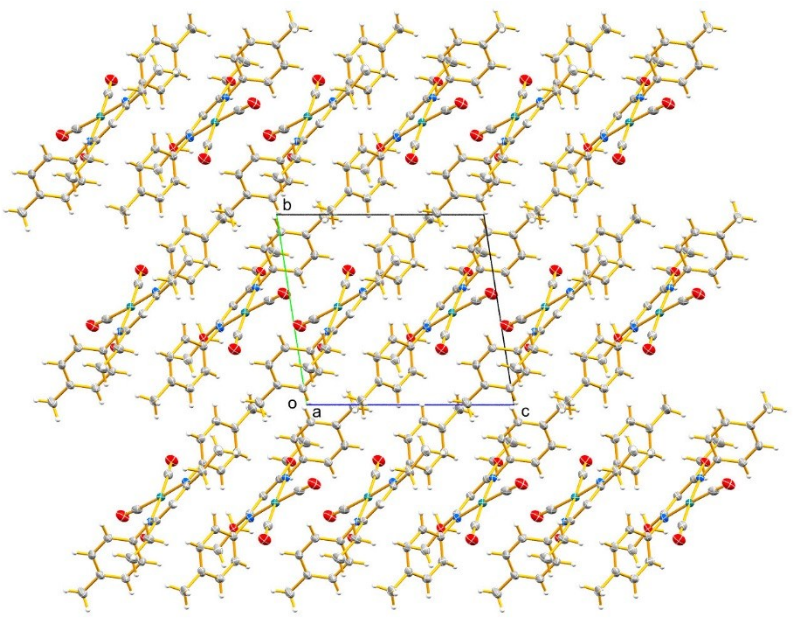

Figure S6: Solid state packing diagram of **11**, viewed down the *X*-axis.

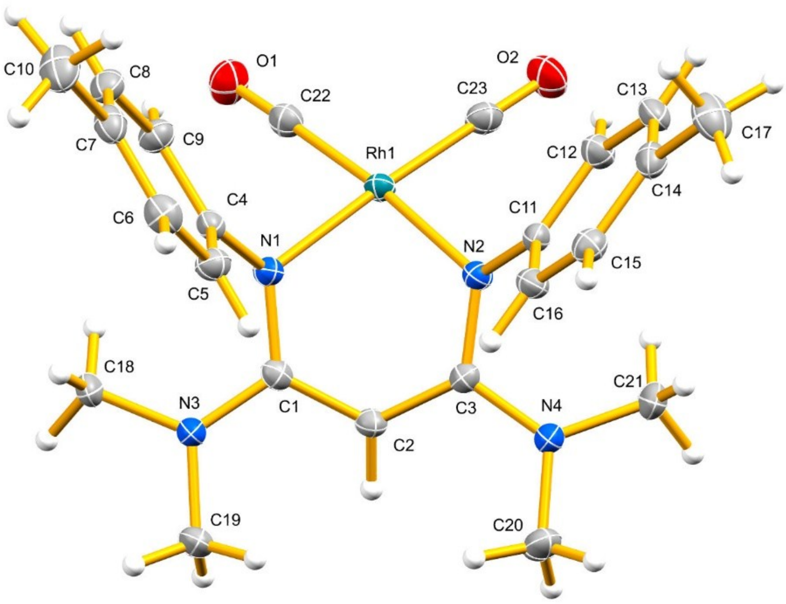

Figure S7: Solid state structure of **12** with all heavy atoms labelled.

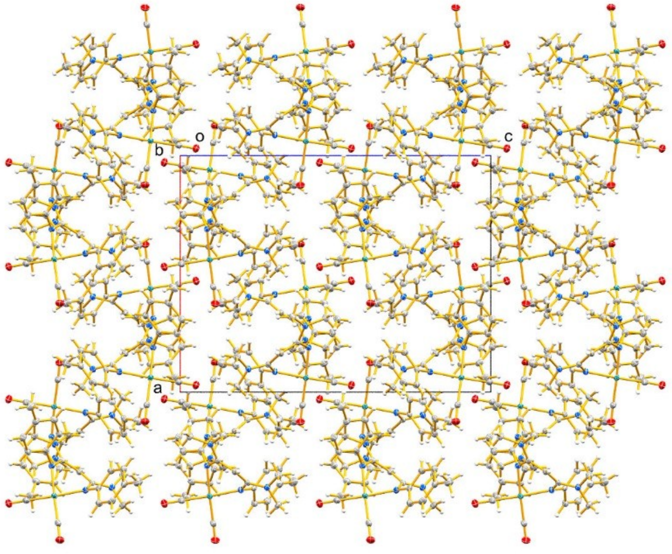

Figure S8: Solid state packing diagram of **12**, viewed down the *Y*-axis.

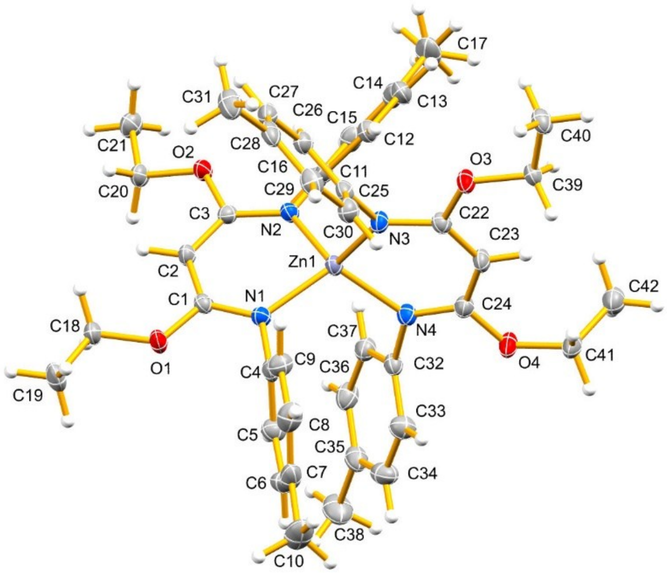

Figure S9: Solid state structure of **15** with all heavy atoms labelled.

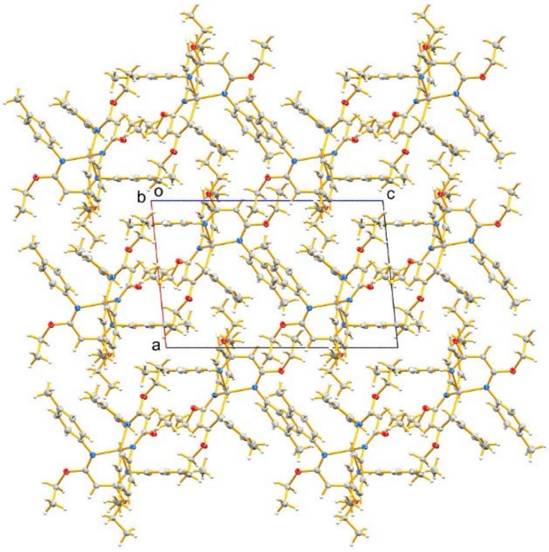

Figure S10: Solid state packing diagram of **15**, viewed down the *Y*-axis.

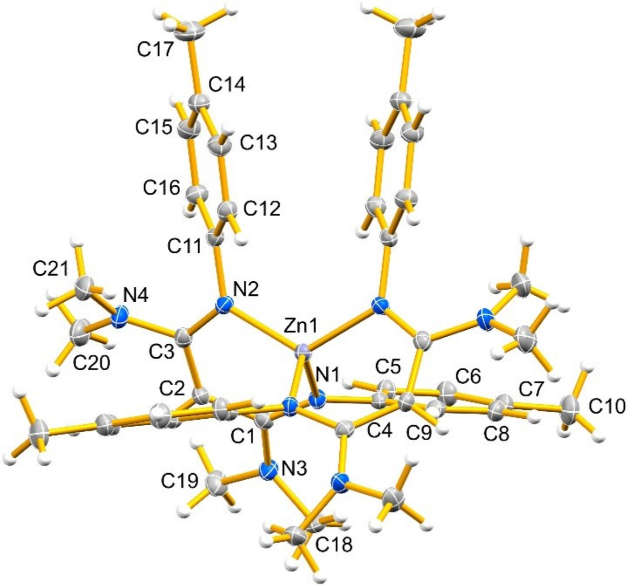

Figure S11: Solid state structure of **16** with all heavy atoms labelled.

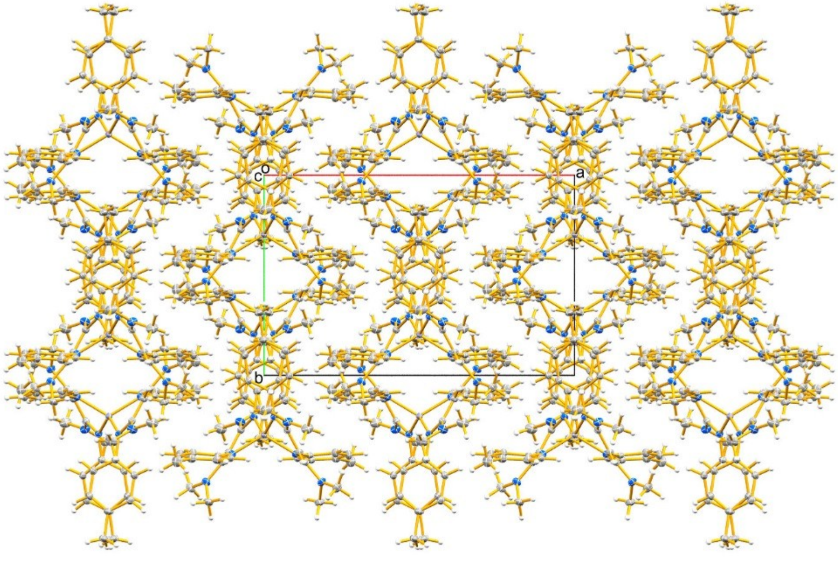

Figure S12: Solid state packing diagram of **16**, viewed down the *Z*-axis.

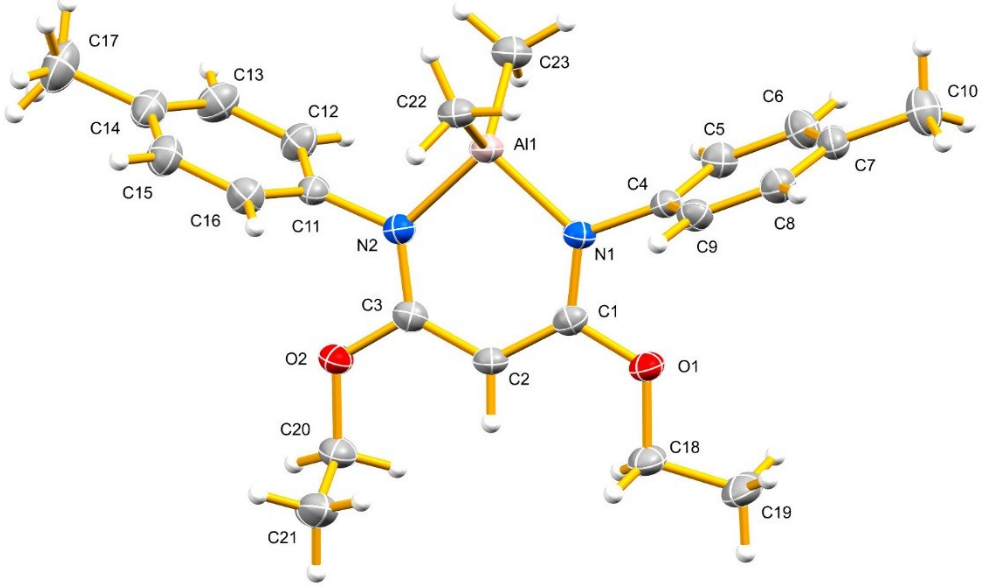

Figure S13: Solid state structure of **17** with all heavy atoms labeled.

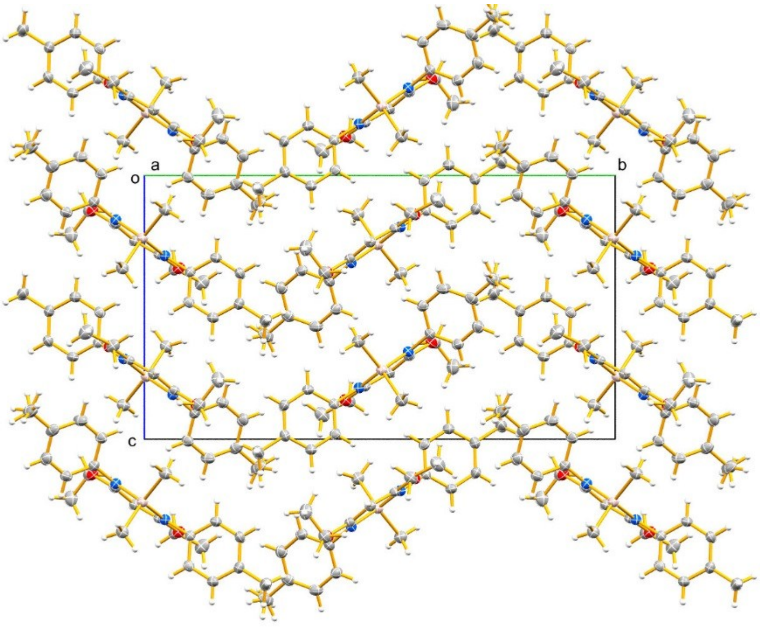

Figure S14: Solid state packing diagram of **17**, viewed down the *X*-axis.

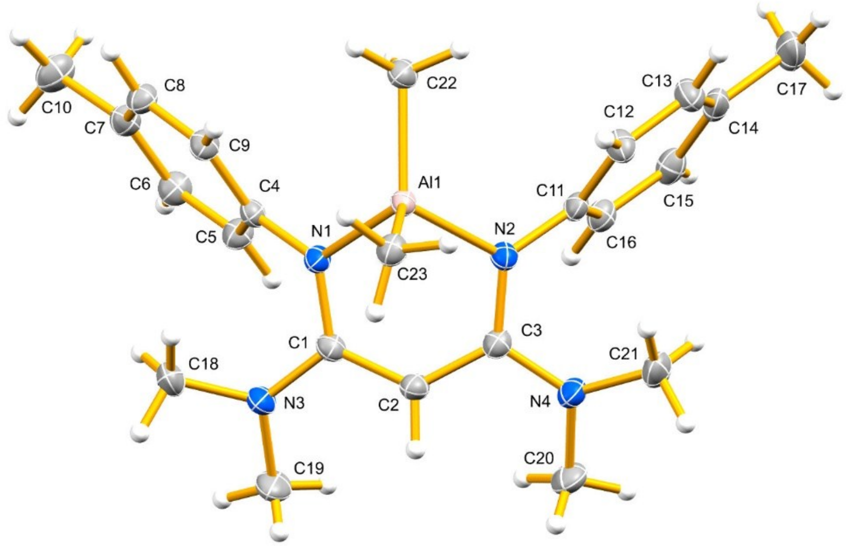

Figure S15: Solid state structure of **18** with all heavy atoms labeled.

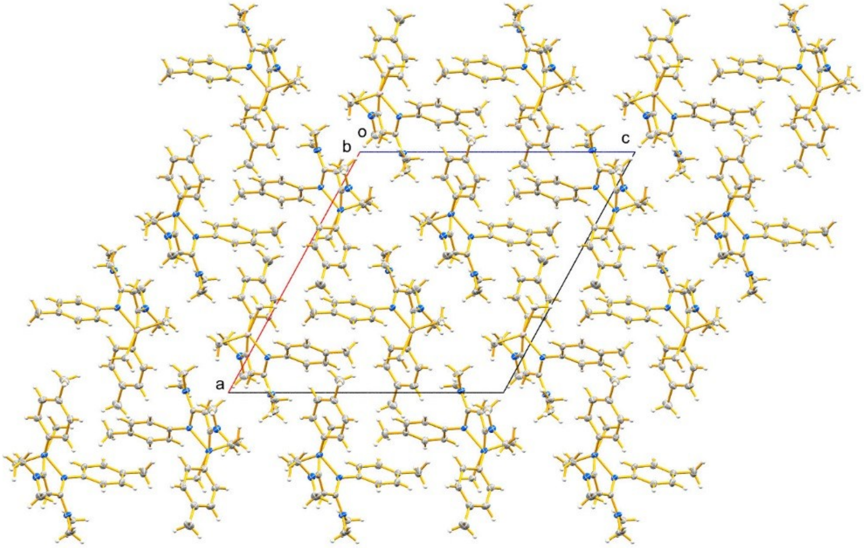

Figure S16: Solid state packing diagram of **18**, viewed down the *Y*-axis.

Additional Crystallographic Discussion:

Intermolecular Interactions of the Ligand Precursors

Compound **5**

There is one intramolecular contact between the two rings [C(12)-H(12)…C(8)] that is shorter than the sum of the van der Waals radii (the cutoff chosen for this work). One of the protons on the central carbon (H2B) is also oriented favorably to form intramolecular contacts with each of the *p*-tolyl rings, interacting with the C(4)-C(5) bond of one ring and with C(11) in the second ring. There are a number of relatively short intermolecular contacts in the structure as well, with both the oxygen and nitrogen atoms acting as acceptors for C-H type hydrogen bonds. In the crystal, these occur at approximately right angles to each other, joining the molecules into a three dimensional network. This network is further supported by one short intermolecular C-H bond from a methyl proton of an ethoxy group to the centroid of a phenyl ring and one short C-H…H-C contact between an ethoxy CH_2 proton and an aromatic proton on one of the *p*-tolyl rings.

Compound **6**

There are few intermolecular interactions in this structure and surprisingly none feature nitrogen as the sole acceptor. Below the limit of the van der Waals radii there are only 4 C-H…H-C contacts and 7 C-H…C intermolecular contacts (only one of which is between the two molecules in the asymmetric unit). The C-H…C contacts have aromatic rings (2), bonds (3), and individual atoms (2) as acceptors. There are many more intramolecular contacts in the structure. In particular, certain methyl protons of the NMe_2 groups are consistently oriented to contact the nitrogen atoms of the backbone. There are also a number of short C-H…H-C and C-H…C intra-type contacts. Of these, the most interesting are the contacts formed between the protons on the central carbon of the backbone in each of the two molecules. These protons lie on either side of a plane through the backbone and thus interact (strongly) with methyl protons of NMe_2 groups that lie on opposite “sides” of the molecule. The same pattern of intramolecular contacts is thus observed in each of the two molecules, but this pattern is quite different from that observed in **5**.

Comparison of the Ligand Precursors to the Coordinated Ligands

Complexation of the ligands forces them to adopt quite different spatial orientations once they are bound to a metal center through the two nitrogen atoms. Changes in the electronic properties of the bound ligands relative to the ligand precursors (loss of H^+) also have an effect on the structural parameters both within and without the backbone. The NC bonds of the ligand backbone are significantly longer, and the CC bonds are significantly shorter in the bound ligands compared to their respective “free” counterparts. The angles at C1 and C3 are somewhat invariant but the angle at C2 is significantly larger when the ligand is bound to a metal, whether it has OEt or NMe_2 substituents. All of this is in keeping with delocalization of charge over the entire ligand backbone and a concurrent change in the hybridization of the central carbon atom from sp^3 to sp^2. The remaining bond lengths and angles are relatively consistent on going from the ligand precursor to the bound ligand, though minor changes are observed in the bonds and angles involving the atoms closest to the backbone. The CO bonds to the OEt groups appear to be very slightly longer and the CN bonds to the NMe_2 groups appear to be very slightly shorter when they are complexed, relative to the respective “free” ligands. This suggests that the NMe_2 groups are more involved in the electron delocalization than are the OEt groups.

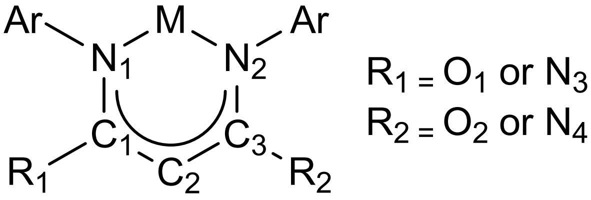

Scheme S1: Atom numbering schemes used for the metal complexes.

Once coordinated to a metal center, the two different ligands can be compared on a general basis. Overall, the NC bonds of the ligand backbone are slightly longer in the NMe_2 complexes relative to their OEt counterparts. The CC bonds are much more similar, but overall, again the bonds in the NMe_2 complexes are slightly longer. The angles at the nitrogen centers in the backbone (involving heavy atoms of the backbone) are much larger in the OEt complexes (~124°) than in the NMe_2 compounds (~116°), and within each set these values are quite consistent. The angles at the carbon atoms of the backbone are also generally larger in the OEt complexes than in the NMe_2 complexes, however, here the differences are not so great (~125° versus ~122°, respectively). In the NMe_2 complexes of Al and Zn the C1-C2-C3 angle is significantly larger (~127°) than the angles at the other carbon atoms of the ligand backbone (~122°).

The longest metal nitrogen bonds (MN) and smallest NMN angles are found in the square planar Rh complexes. The tetrahedral Al and Zn complexes have similar NMN angles but the NM bonds are slightly longer in the Zn complexes.

Once coordinated, the planarity of the ligands can vary significantly. Overall, the *nacnac*^{OEt} complexes have much more planar ligands than the *nacnac*^{NMe2} complexes. In fact, the metal-ligand ring in the Al ethoxy complex is virtually planar while all of the NMe_2 complexes have metal-ligand rings that are significantly puckered. The same evidence is obtained if one looks at the deviation of the metal atom from the ligand plane defined using the atoms N1, N2, C1, C2 and C3 in each case. The metal atom always lies much further out of the defined "plane" in the NMe_2 complexes (0.847(2) to 1.233(2) Å) compared to the OEt complexes (0.116(2) to 0.279(2) Å). In terms of the metal center, the Rh complexes are significantly less planar than the Al or Zn complexes, where the deviations of the metal center from the ligand planes are quite similar.

The ligands both appear to have a large range of functional flexibility. This is evident in the wide range of N…N distances (between the two nitrogen atoms bound to the metal center) adopted in the various complexes. In the NMe_2 complexes, this distance is 2.751(2) Å in the Rh complex and 2.959(2) Å in the Zn complex. For one metal, the largest difference between the two ligands is seen in the Rh complexes, where the OEt compound has an N…N distance of 2.904(2) Å.

The phenyl rings of the ligands in all of the complexes are always planar. The orientation of the two phenyl rings on each bound ligand type is also quite consistent (with one notable exception). In general, the phenyl rings of the OEt complexes have interplanar angles of between 44 and 53° (average 48°). Two of the NMe_2 complexes also have angles that are close to one another, the Rh complex angle being 73.80(6)° and that of the Zn complex, 77.59(6)° (average 76°). The NMe_2 phenyl ring planes are thus generally rotated away from each other by ~28° more than are the planes in the ethoxy complexes. The one significant outlier from this pattern is the Al NMe_2 complex, where the angle between the phenyl ring planes of 85.12(4)° is ~10° larger than the NMe_2 average. This large change in the orientations of the phenyl rings in the Al complex must arise from the fact that the $Al(Me)_2$ fragment has rotated down towards the ligand plane in this structure (see Figure S16).

The ligand groups (OEt and NMe_2) have quite characteristic conformations in these complexes. In particular, the ethoxy ligands are noteworthy. These ligands always adopt one of two possible geometries, sometimes both in the same structure, although the factors influencing their positions are not entirely clear. The OEt groups are always oriented either parallel (ranging from 2.8(2)° in the Rh complex to 13.5(2)° in the Zn complex) or perpendicular (87.1(1) in Al to 90.0(1)Å in Zn) to the plane of the ligand. This means of course that that they are also always perpendicular or parallel to each other. The parallel arrangement of the ligand is the more common, while the perpendicular orientation is seen only in one of the two OEt groups on the Al complex and one of four on the Zn complex. The perpendicular arrangement of OEt groups is also that found in the structure of the free ligand precursor.

The arrangement of the NMe_2 groups in those complexes is quite different, from both the OEt structures and from each other. The angle between the two groups steadily increases in the order Rh (10.7(3)°), Al (24.3(2)°), and Zn (43.5(2)°). The angle of each NMe_2 group to the ligand plane is similar in all of the compounds, but this too gradually increases from ~20° in the Rh to ~22° in the Al and to ~28° in the Zn complex. This could be related to the size of the metal centers and the geometries the ligands are forced to adopt when binding to them, as the angles do increase in order from largest to smallest.

Intermolecular Interactions and Contacts in the Metal Complexes

In all of the structures discussed, only contacts below the level of the van der Waals' cutoff (less than the sum of the vdW radii of the interacting atoms) will be considered.

There is very little participation of the metals in the different structures in forming intermolecular contacts. Only rhodium was found to act as a contact acceptor and in each structure (OEt and NMe_2) only one such contact was observed. Somewhat surprisingly, very few interactions were observed with the N or O atoms of the ligands acting as acceptors and there was no particular pattern observed for such contacts. There are a variety of aromatic-type carbon atoms in the ligands that can participate in interactions (the ligand backbone, phenyl rings, aromatic bonds, or individual atoms). This type of interaction, C-H…C, is observed in all of the structures but a few general observations are possible. Overall, there are significantly more C-H…C contacts in the NMe_2 complexes compared to the OEt solids. These tend to be intramolecular in nature, and tend to involve methyl protons of the NMe_2 groups interacting with phenyl rings (ring, bond or atom) as acceptors. Only the zinc ethoxide structure has more than one or two C-H…C contacts, and all but one of these involve protons of the ethoxy groups as donors.

Finally, and again surprisingly, each structure participates in only a limited number of C-H…H-C type contacts and most of these tend to be intramolecular. As an overall group, only one proton stands out in every structure studied. The C-H proton on the central carbon of the ligands is always involved in short, intramolecular C-H…H-C contacts. These contacts differ depending on the ligand, but are consistently observed within each ligand group. In the Al and Zn NMe_2 compounds, this C-H interacts with methyl protons from NMe_2 groups lying on opposite sides of the molecule (groups on either end of the ligand backbone). There are short interactions with 2 different protons of each methyl group for a total of 4 short C-H…H-C contacts involving this hydrogen. In the rhodium structure the contacts are related but slightly different. The NMe_2 methyl groups no longer have the protons aligned such that two protons from each group can interact with the central C-H. Instead only a single proton from each methyl group interacts (still on either side of the molecule) and there is a third, longer, intermolecular contact to a phenyl proton on the backside of the molecule.

The contacts of the central ligand proton in the ethoxy compounds are even more interesting. Here, the contacts formed are always intramolecular in nature but they also depend exclusively on the orientation of the ethoxy groups in the structure. If an ethoxy group lies in the plane of the ligand, then this H forms contacts with each of the protons on the CH_2 group of that ethoxy. However, if the ethoxy group is oriented perpendicular to the ligand plane, then the contacts formed are different. The central hydrogen still interacts with one proton from the ethoxy CH_2 group (now an even shorter contact), but it also interacts with one proton from the methyl group of the same ethoxy (as a slightly longer contact). This distribution of contacts is identical in all of the compounds studied and could be used to identify the configuration of the ethoxy groups in the absence of a diagram. Every ethoxy group interacts with the central proton of the ligand in one of these two ways and there are always 4 C-H…H-C contacts per ligand C-H.

Ring stacking interactions are not prevalent in these complexes. Only the Zn NMe_2 complex **16** has an interaction of less than 4.4 Å and it, at 3.888(1) Å, is unlikely to be very important. Of note, this contact is intramolecular, occurring between two halves of the same molecule (where one half is related by symmetry to the other). It likely occurs because of the geometry forced by the NMe_2 groups on the ligand, since the related OEt complex has no stacking contacts below 4.4 Å.

The only other intramolecular interactions of note are found in the $Rh(CO)_2$ complexes (Figure S1). The CO groups in these structures participate fully in the interactions formed. In the ethoxy compound **11**, there is actually a short intermolecular interaction between two O3 atoms of CO groups in adjacent molecules related by symmetry. The distance of 2.869 Å is well below the van der Waals' cut-off. In addition, each CO group is aligned to lie directly above, and form an intermolecular interaction with, the entire phenyl ring lying directly below it in the molecule.

The distance from O3 to the centroid of phenyl ring 1 [C4 to C9] is 3.297(2) Å, while that from O4 to the centroid of phenyl ring 2 [C11 to C16] is 3.589(2) Å; the corresponding C-O…centroid angles are 80.10(11) and 76.15(11)°, respectively. The importance of these interactions to the solid state structures observed is not known. However, the changes observed on going from the OEt to the NMe_2 structure do suggest that these interactions do confer some benefit to the molecule. In the NMe_2 compound **12**, sterics result in the ligand having to adopt quite a different geometry relative to the ethoxy compound. The phenyl rings are now rotated down and away from the $Rh(CO)_2$ region of the molecule and interactions of the type formed in the ethoxide are no longer possible. Instead, a different type of interaction is formed between each of the phenyl rings and the CO group lying nearest it in the molecule. One C-H proton from each phenyl ring forms an intramolecular contact with the CO lying directly above it, giving a C-H…CO contact on each side of the molecule. The fact that such contacts arise in quite different ways in each molecule suggests that they do play a role in stabilizing the solid state.

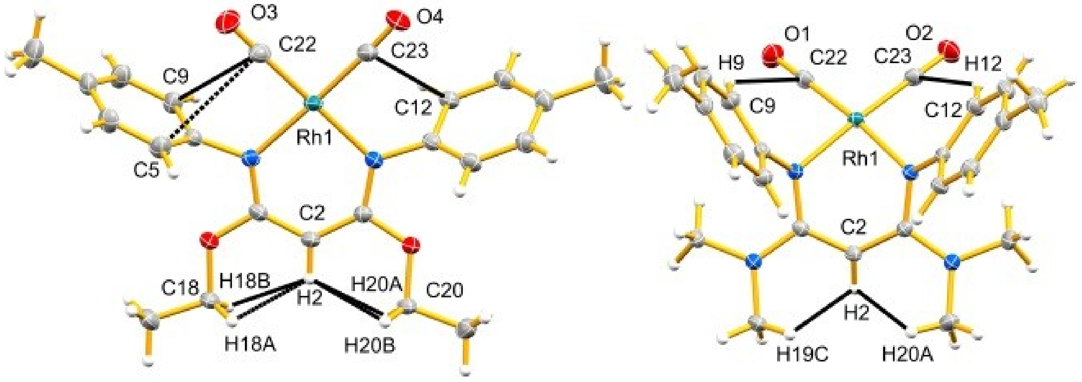

Figure S17: Selected intramolecular contacts (dashed lines) found in the Rh(CO)$_2$ complexes **11** (left) and **12** (right).

Spectroscopy of Compounds

The infrared spectra were obtained using either an attenuated total reflection (ATR) adapter on a Bruker Alpha Spectrometer or as KBr pellets using a Bruker Vertex 70 Infrared Spectrometer. Data processing was completed using OPUS 6.0 software suite and the spectra were plotted with Microsoft Excel 2013. The NMR experiments were carried out on either a Bruker Ultrashield 300 MHz NMR spectrometer with a 7.05 Tesla magnet or on a Bruker AV 500 MHz Spectrometer, with an 11.74 Tesla magnet, at the Nuclear Magnetic Resonance Research Resource (NMR-3) facility at Dalhousie University in Halifax, Nova Scotia. ^{1}H and ^{13}C{^{1}H} spectra were referenced to residual solvent downfield of tetramethylsilane. The data was processed using Bruker TOPSIN 1.3 and the spectra were plotted with ACD/NMR Processor 12.0, Academic Edition.

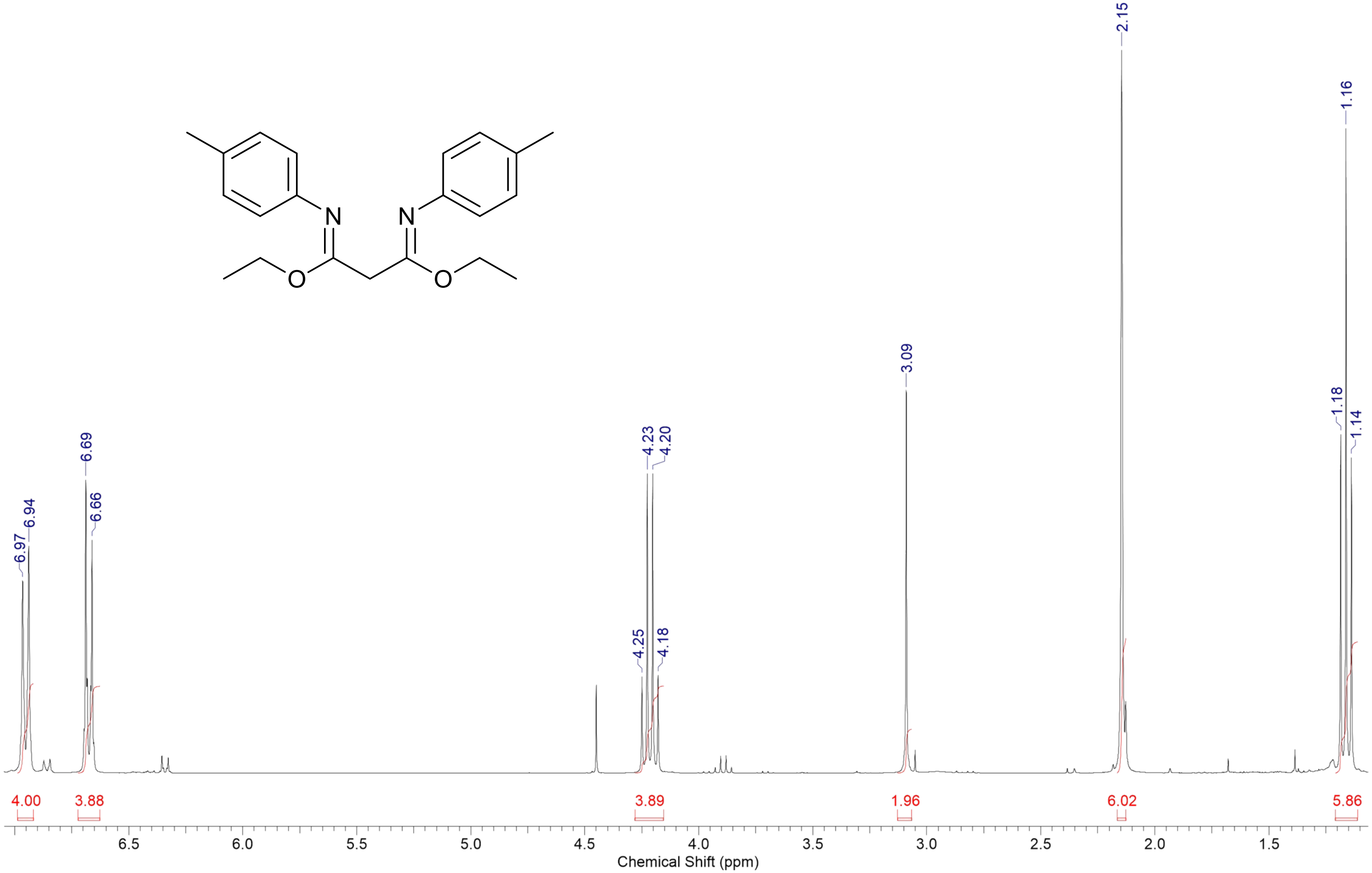

Figure S18: ^{1}H NMR spectrum of **5**, in C_6D_6.

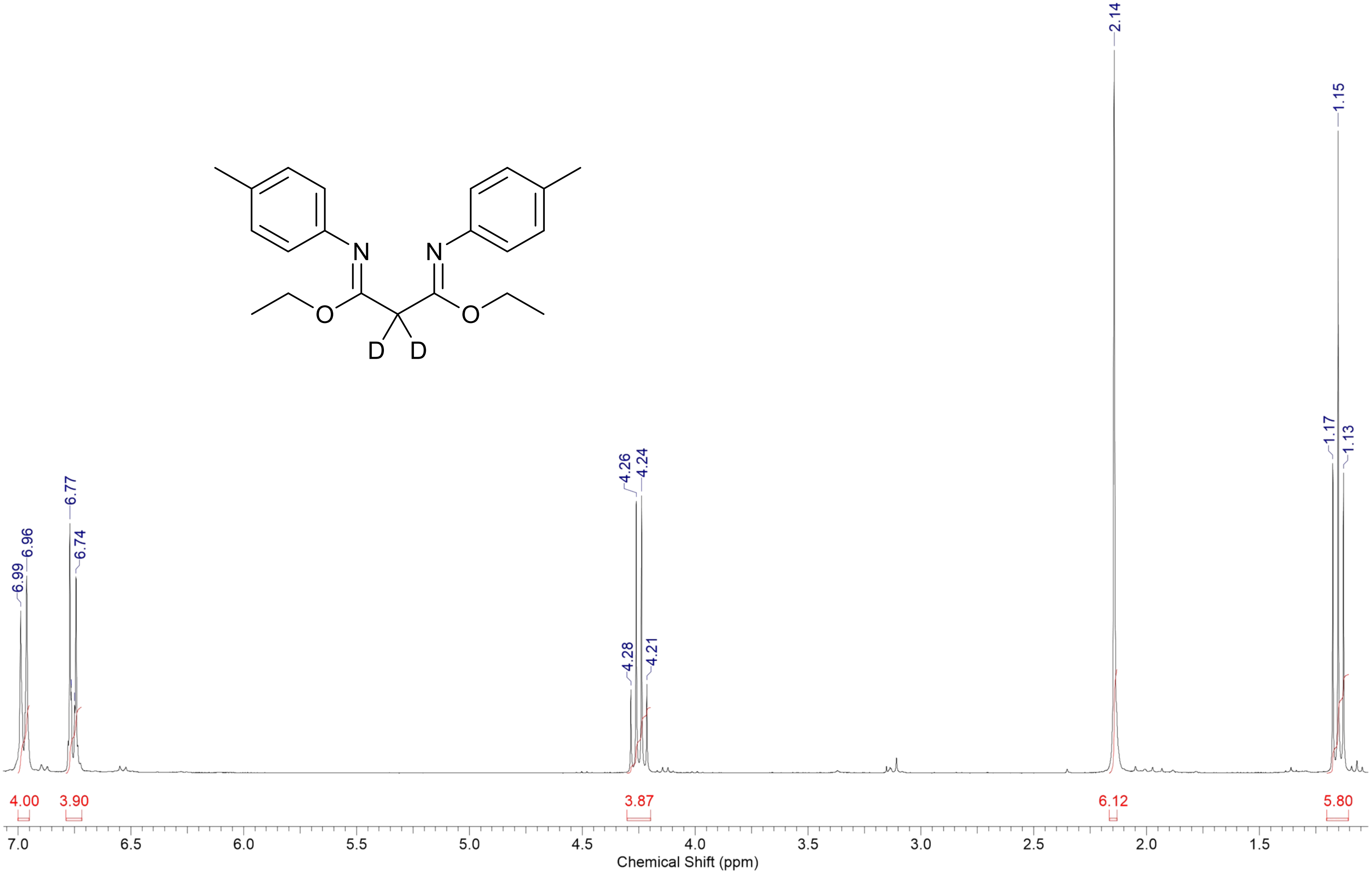

Figure S19: ^{1}H NMR spectrum of **5**-D_2, in C_6D_6.

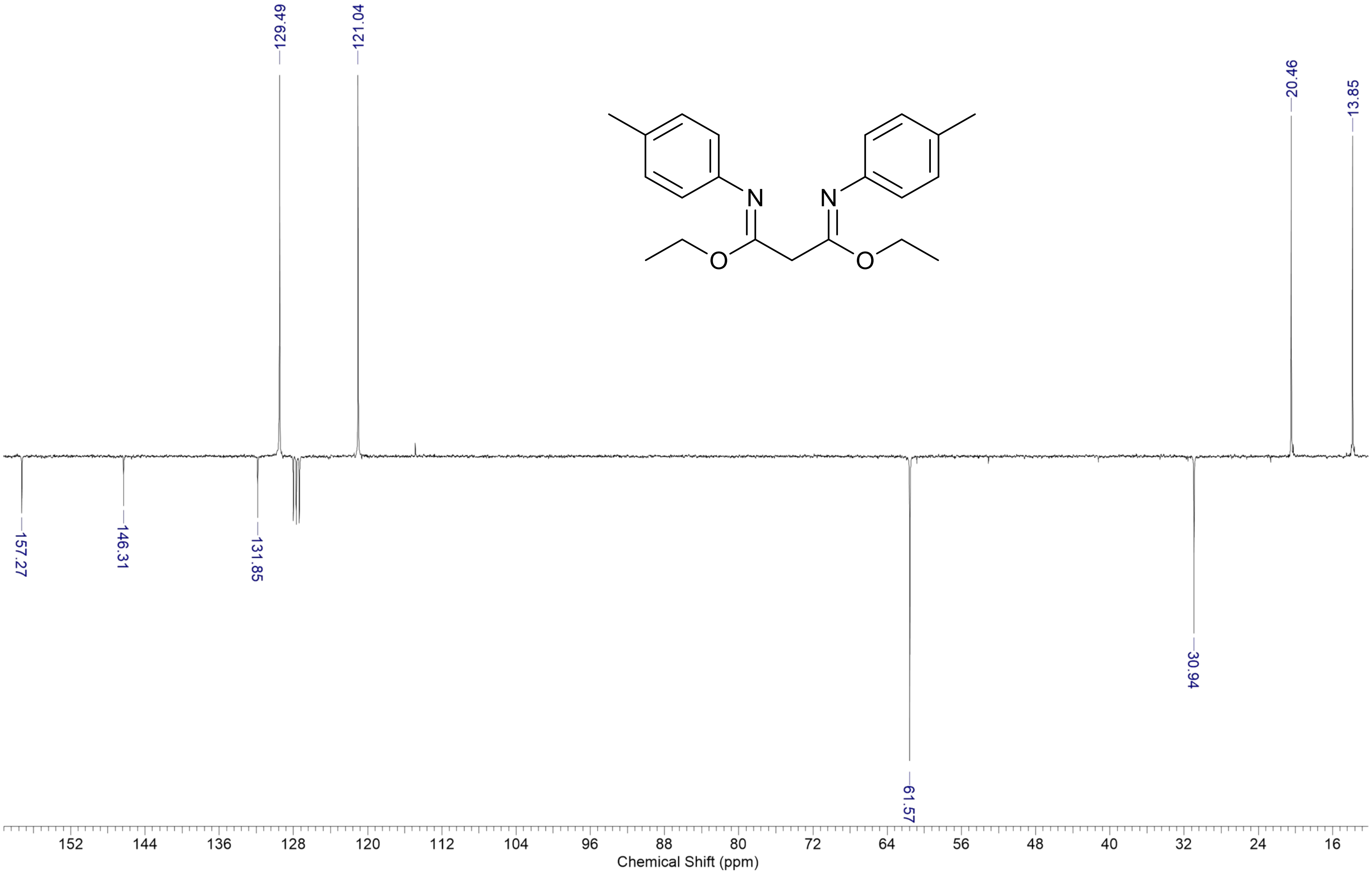

Figure S20: $^{13}C\{^1H\}$ DEPTQ NMR spectrum of **5**, in C_6D_6 (CH & CH_3 ↑, C_q & CH_2 ↓).

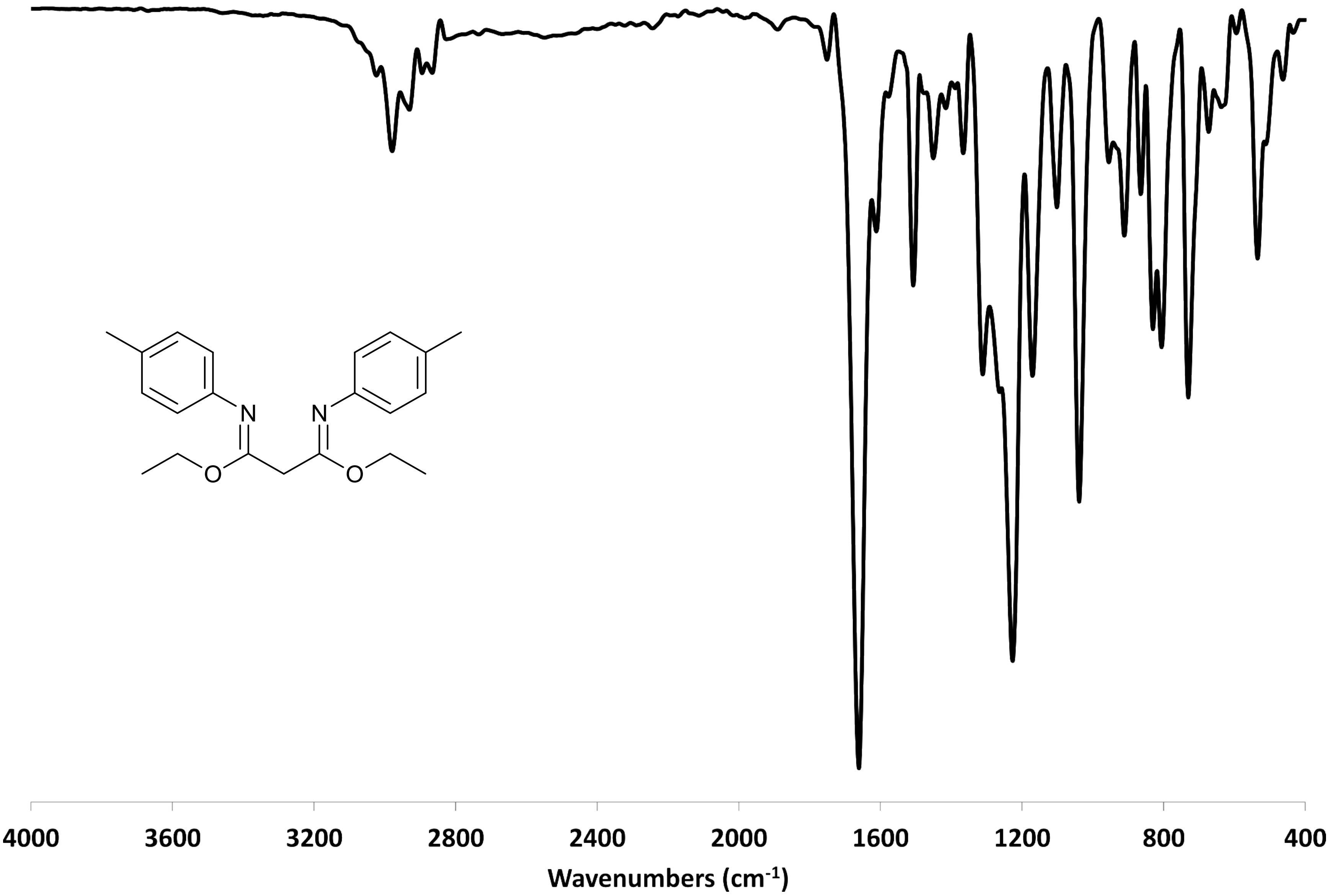

Figure S21: IR spectrum of **5**, obtained by ATR.

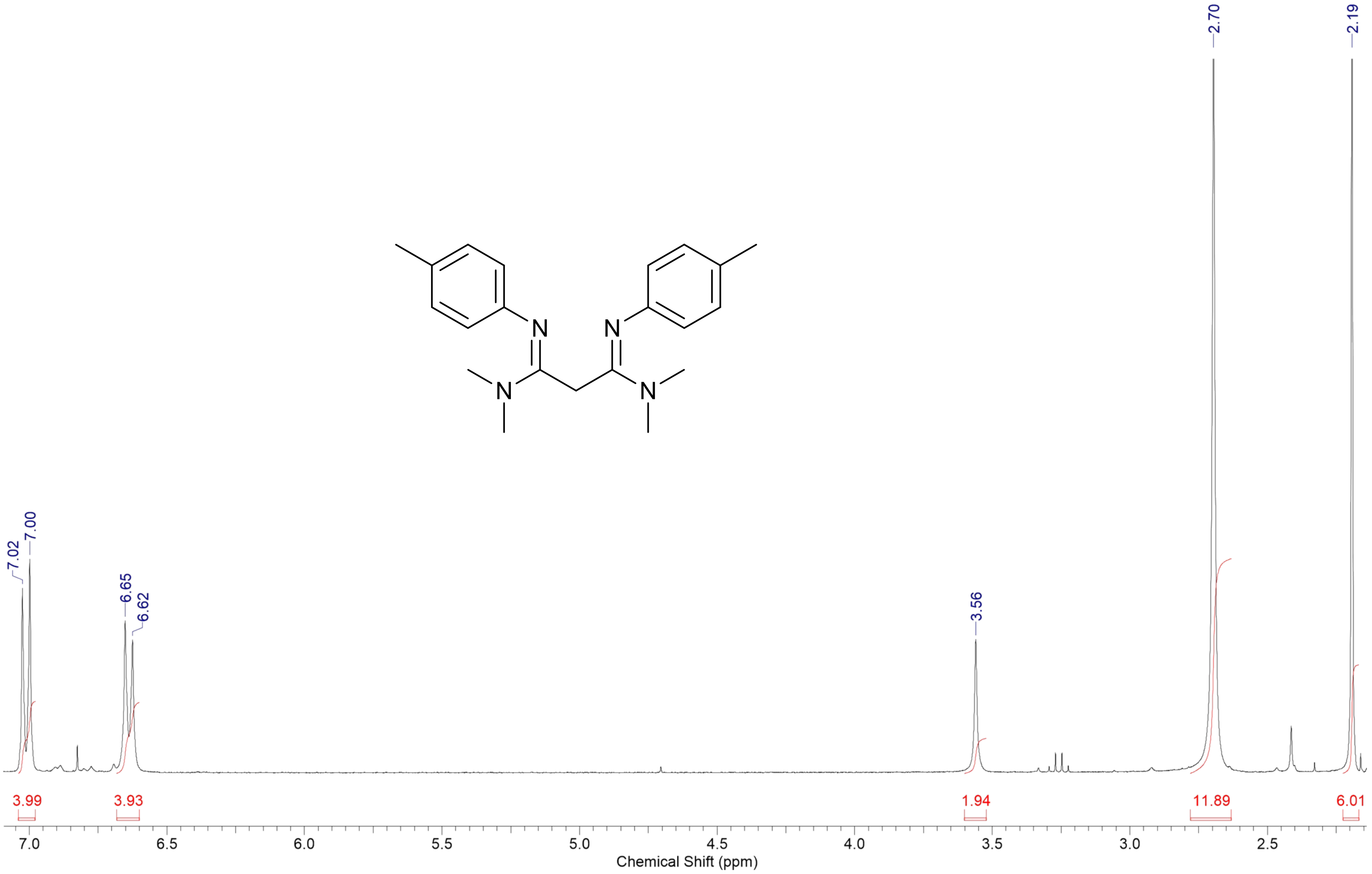

Figure S22: ^{1}H NMR spectrum of **6**, in C_6D_6.

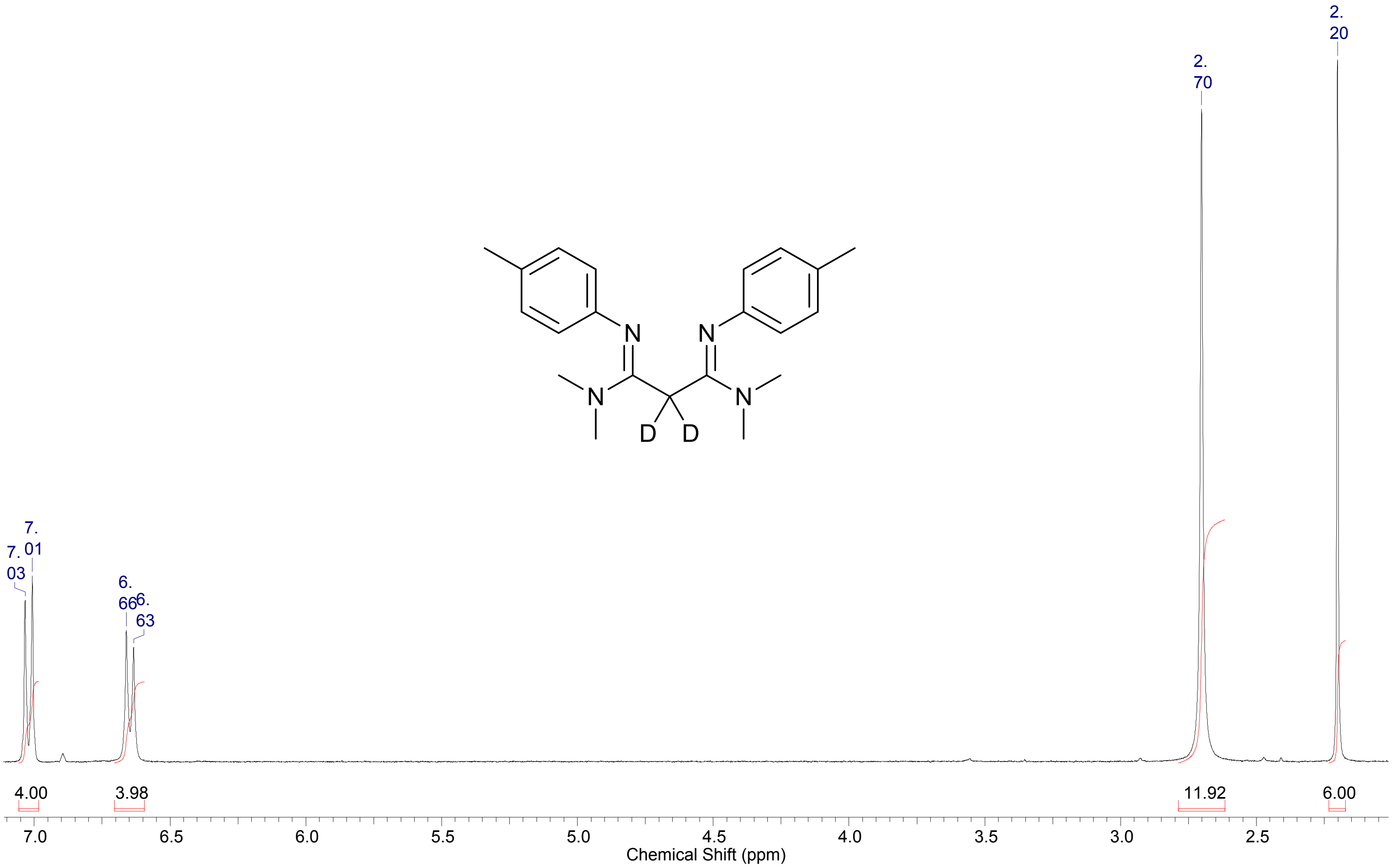

Figure S23: ^{1}H NMR spectrum of **6**-D$_2$, in C$_6$D$_6$.

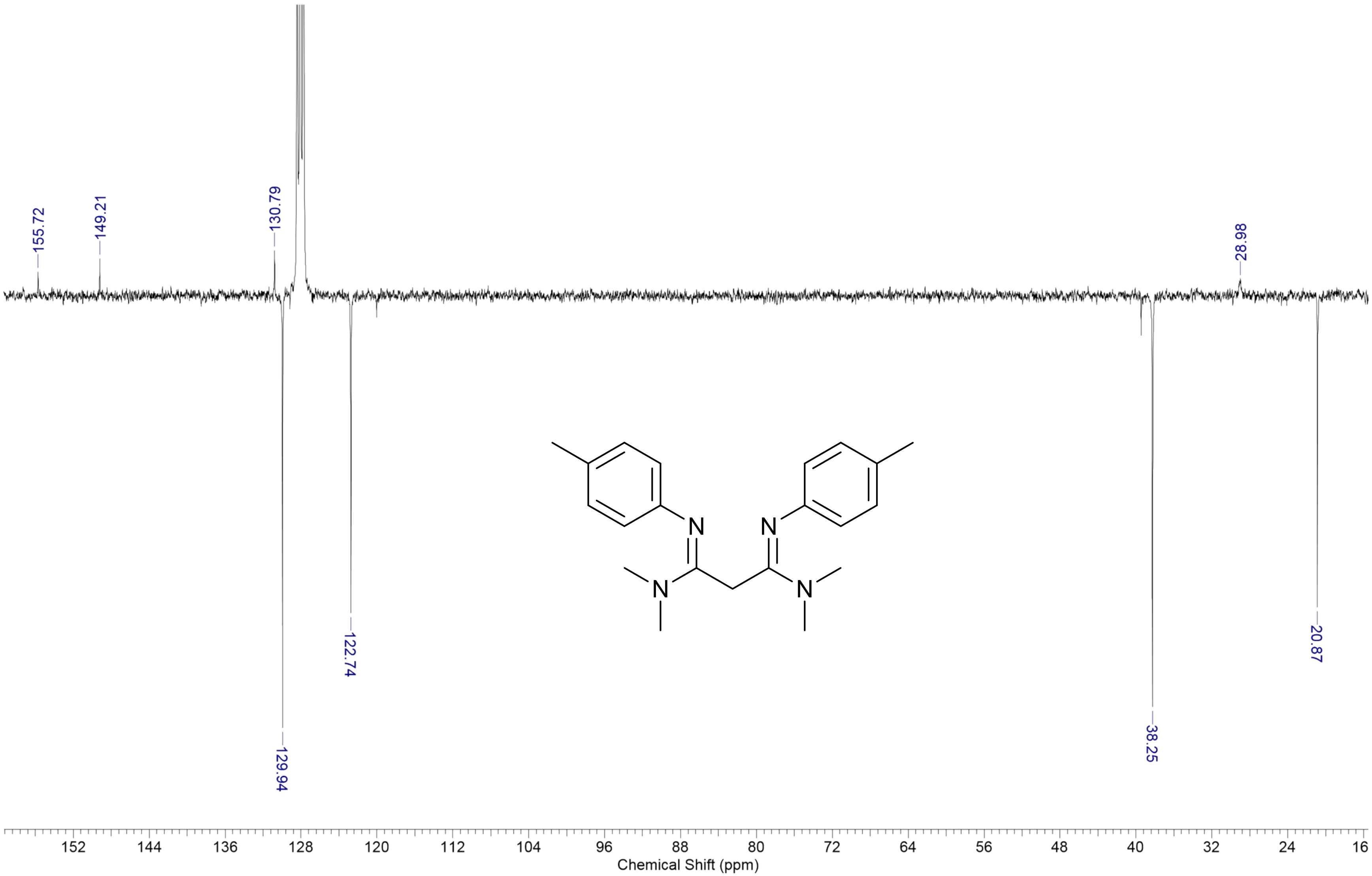

Figure S24: $^{13}C\{^1H\}$ DEPTQ NMR spectrum of **6**, in C_6D_6 (C_q & CH_2 ↑, CH & CH_3 ↓).

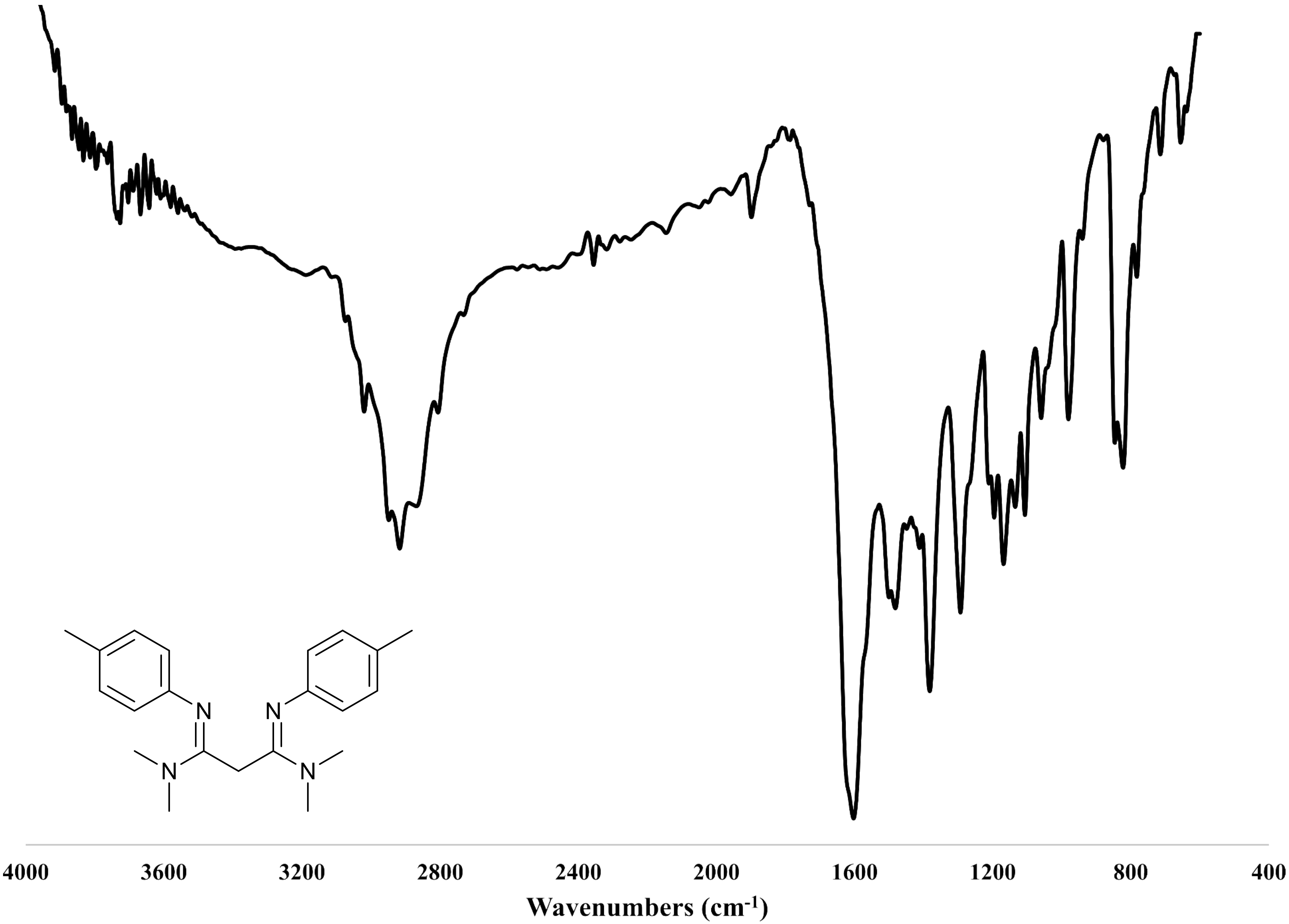

Figure S25: IR spectrum of **6**, obtained as a KBr pellet.

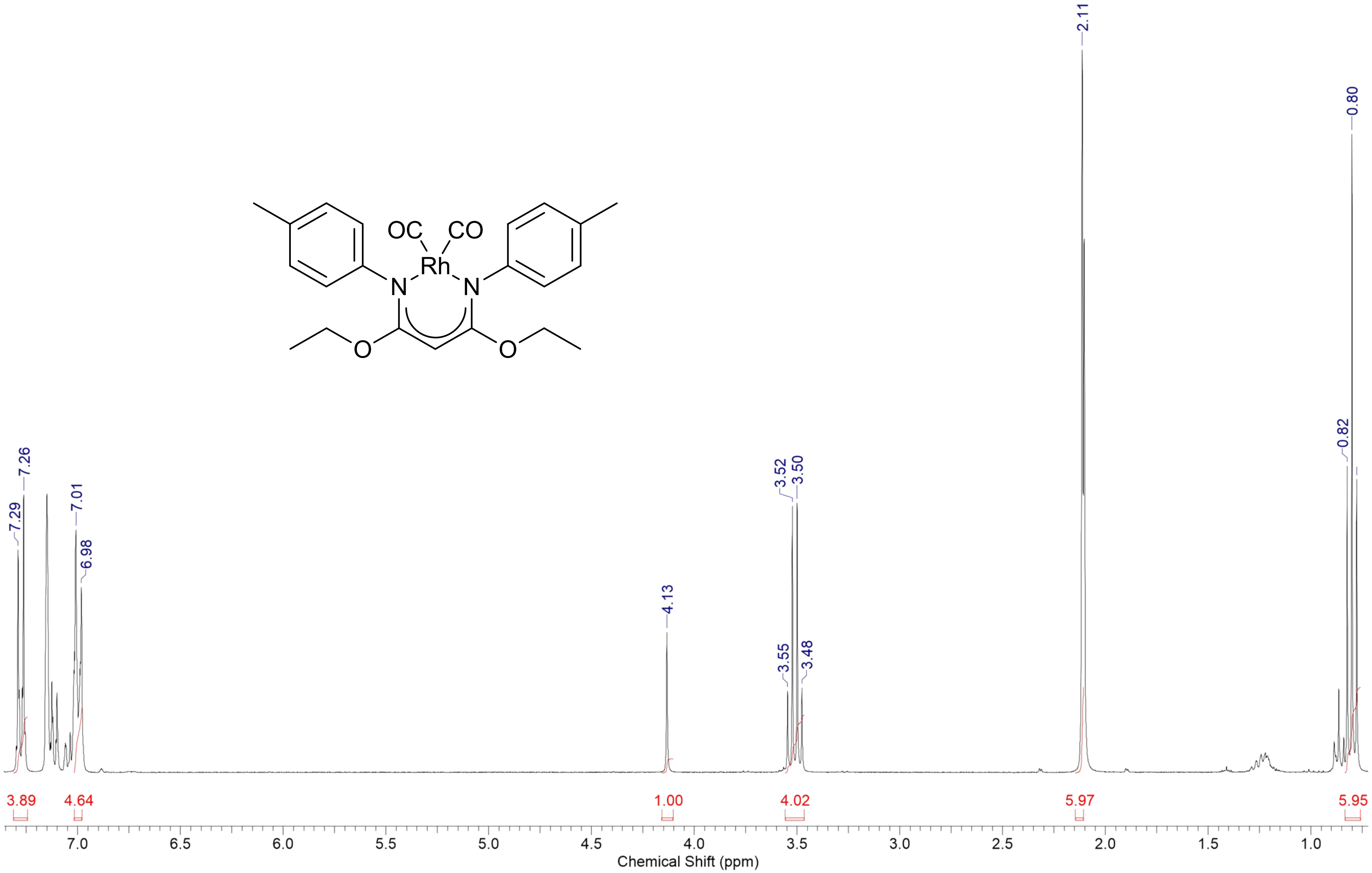

Figure S26: ^{1}H NMR spectrum of **11**, in C_6D_6. Residual toluene is present.

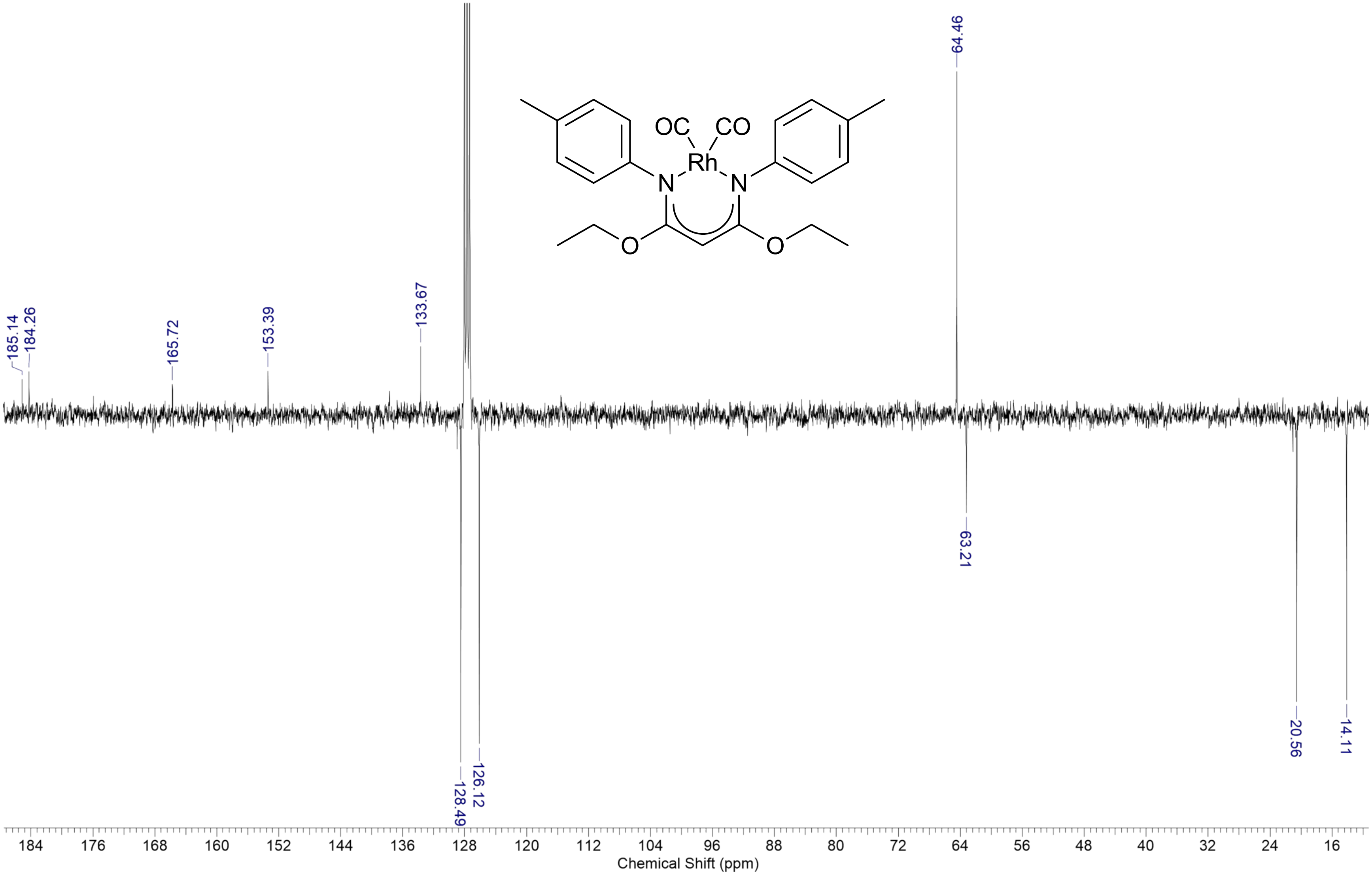

Figure S27: $^{13}C\{^1H\}$ DEPTQ NMR spectrum of **11**, in C_6D_6 (C_q & CH_2 ↑, CH & CH_3 ↓).

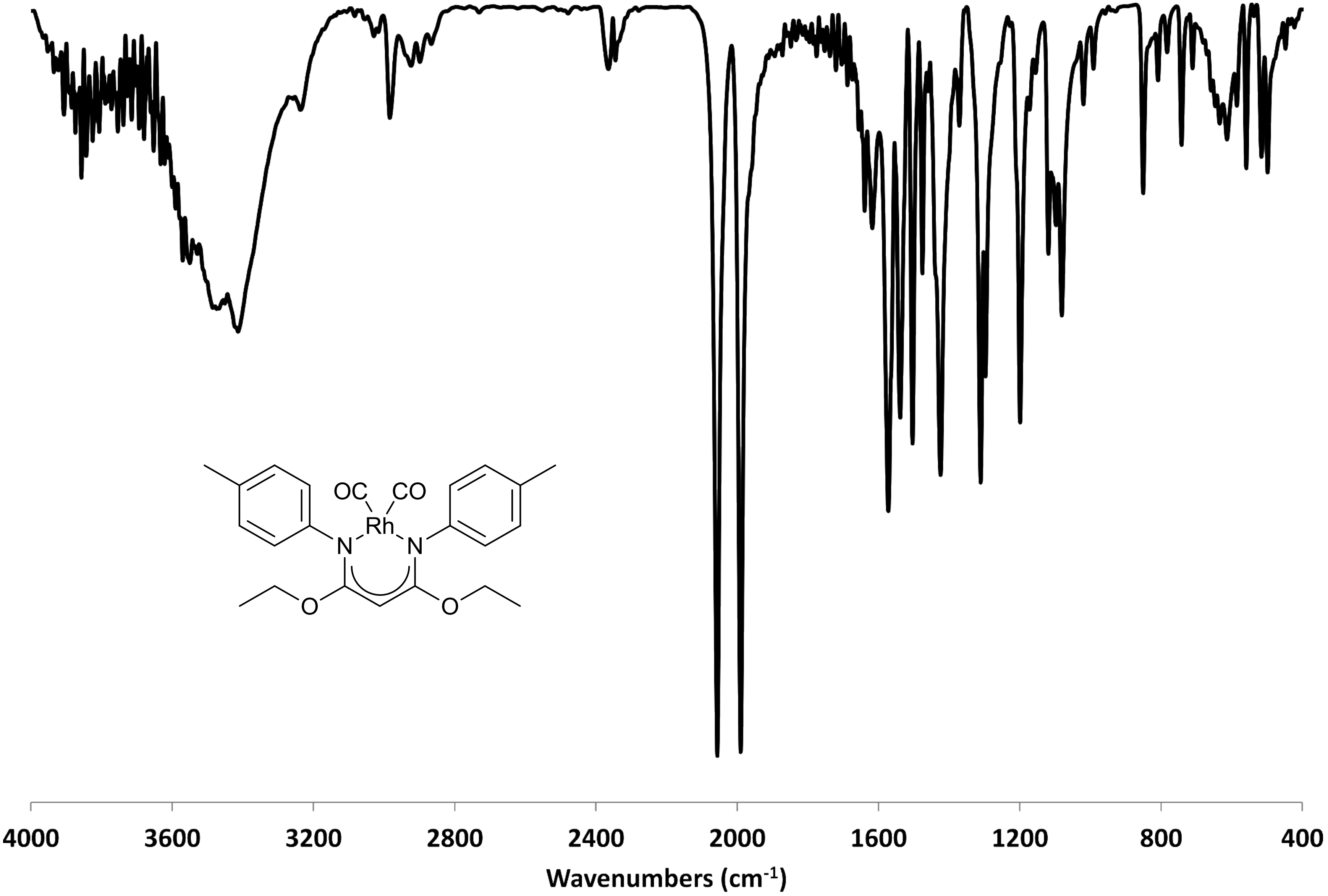

Figure S28: IR spectrum of **11**, obtained as a KBr pellet.

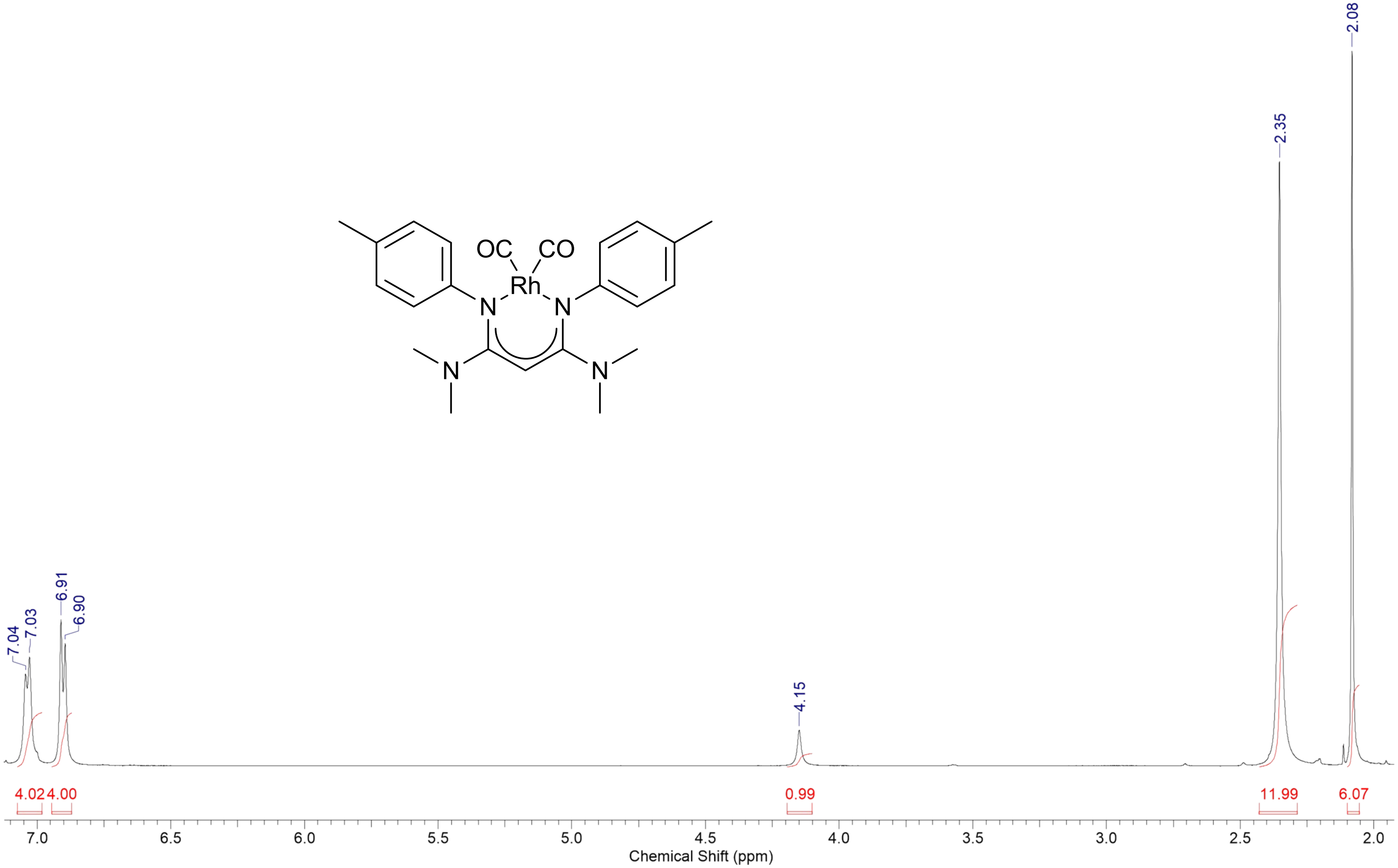

Figure S29: ^{1}H NMR spectrum of **12**, in C_6D_6.

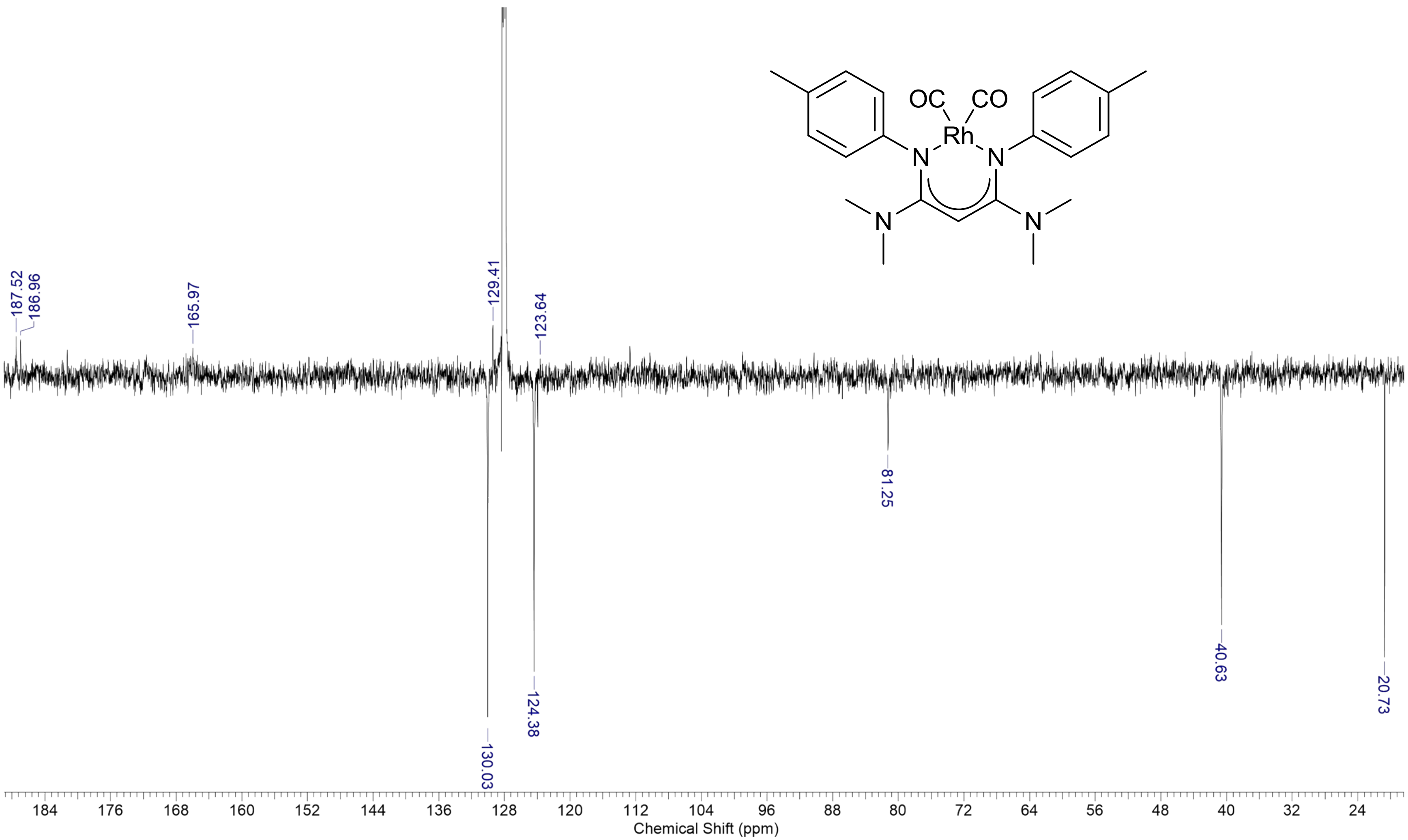

Figure S30: $^{13}C\{^{1}H\}$ DEPTQ NMR spectrum of **12**, in C_6D_6 (C_q & CH_2 ↑, CH & CH_3 ↓).

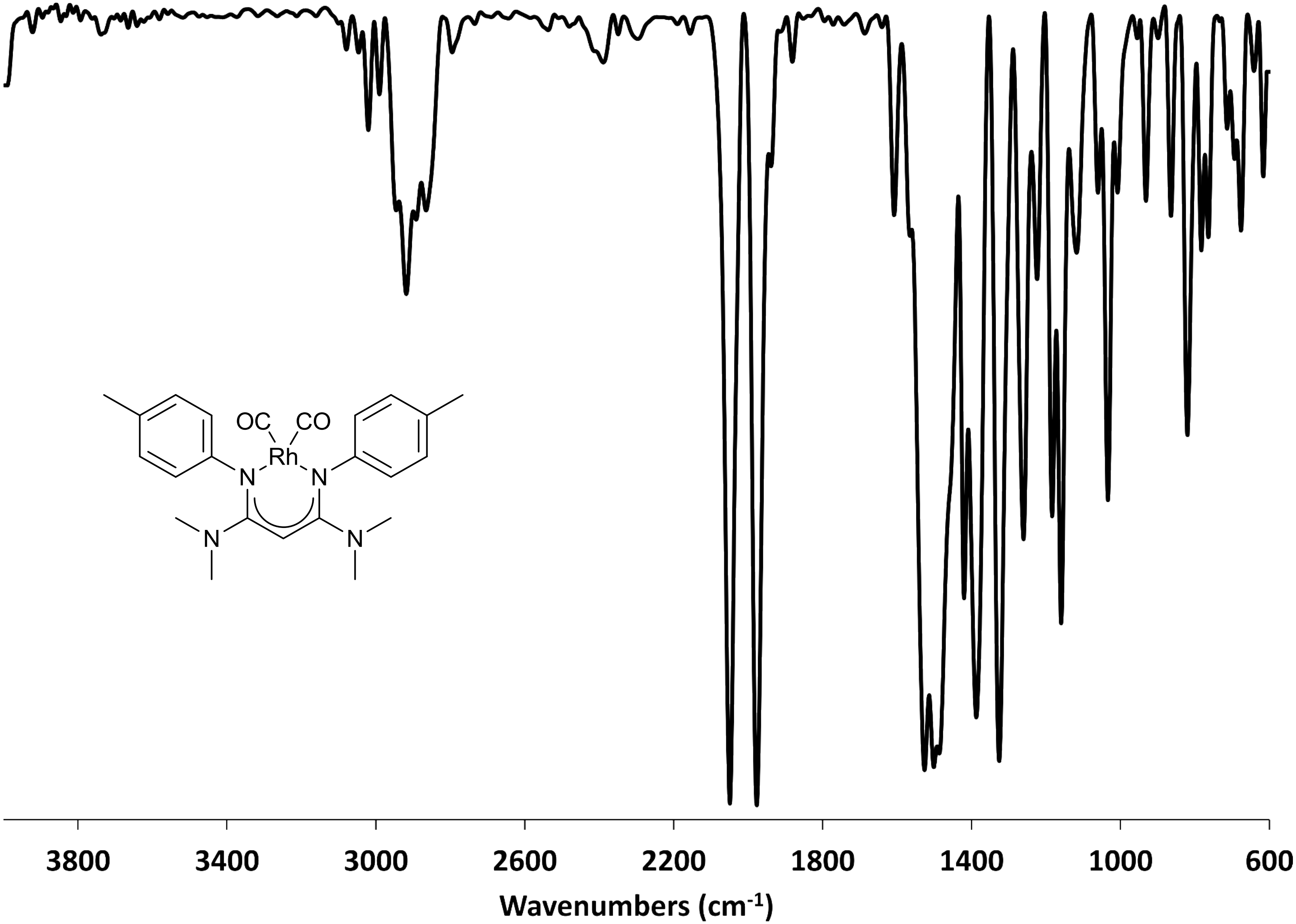

Figure S31: IR spectrum of **12**, obtained as a KBr pellet.

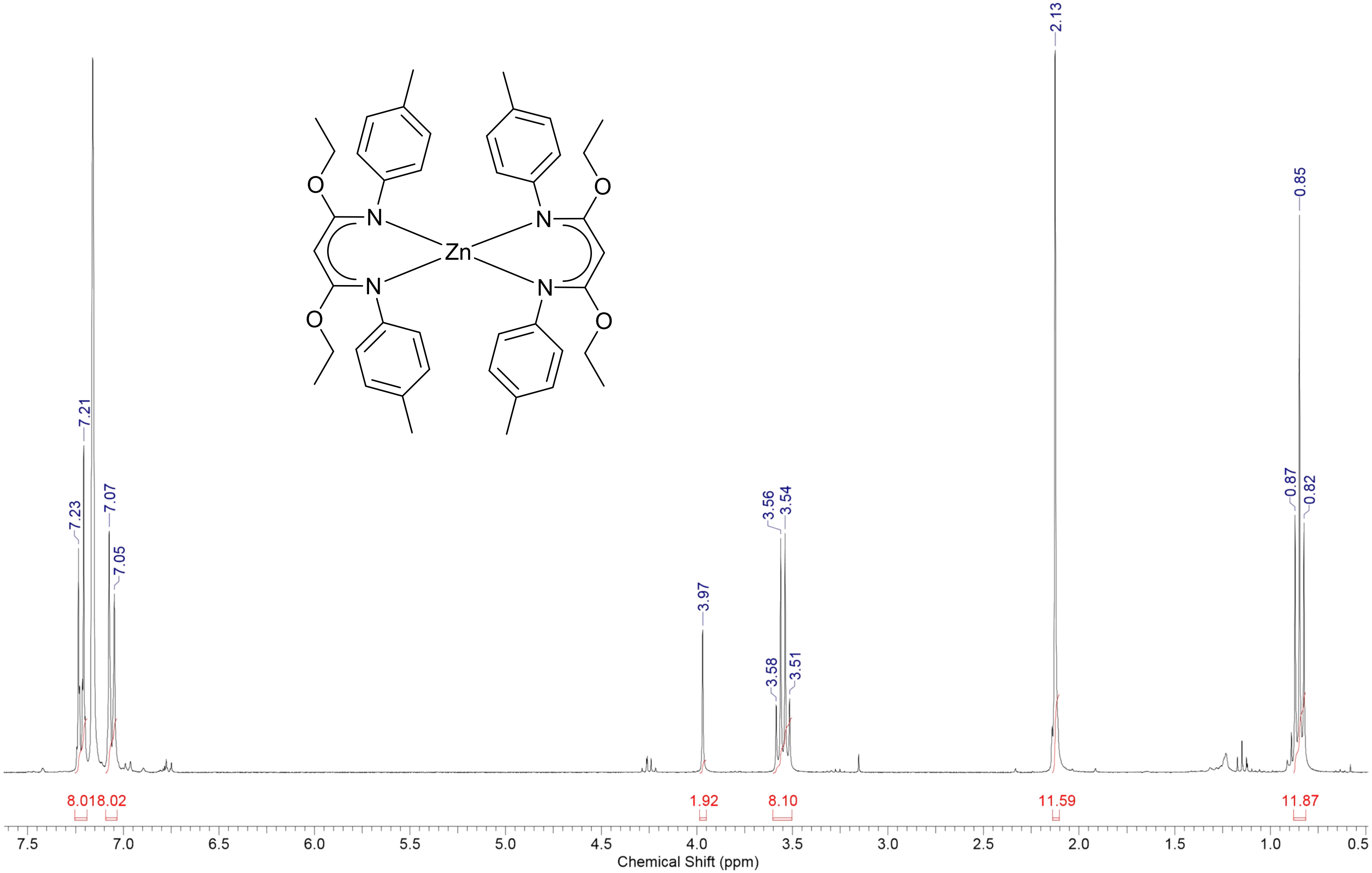

Figure S32: ^{1}H NMR spectrum of **15**, in C_6D_6.

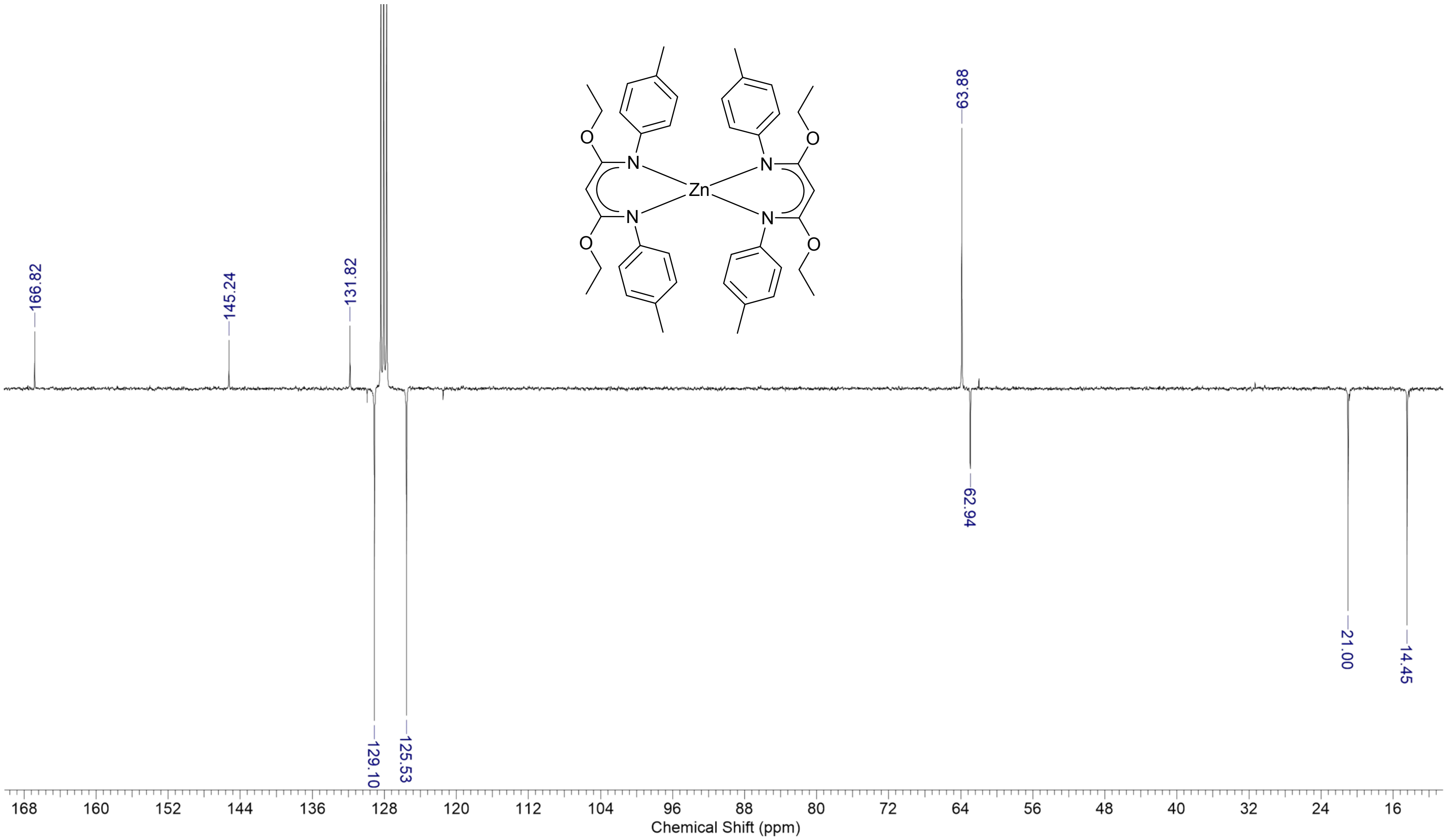

Figure S33: $^{13}C\{^{1}H\}$ DEPTQ NMR spectrum of **15**, in C_6D_6 (C_q & CH_2 ↑, CH & CH_3 ↓).

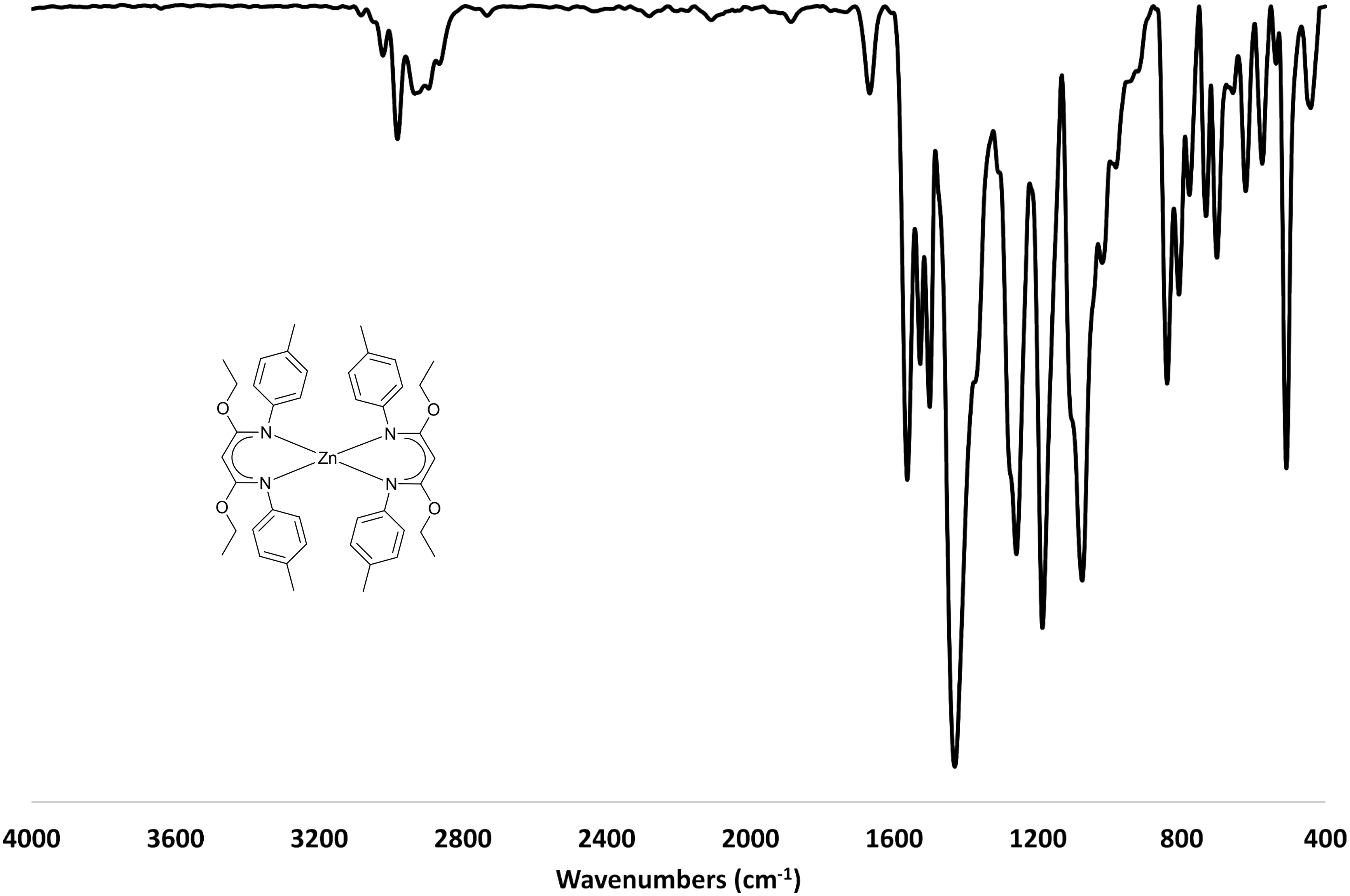

Figure S34: IR spectrum of **15**, obtained by ATR.

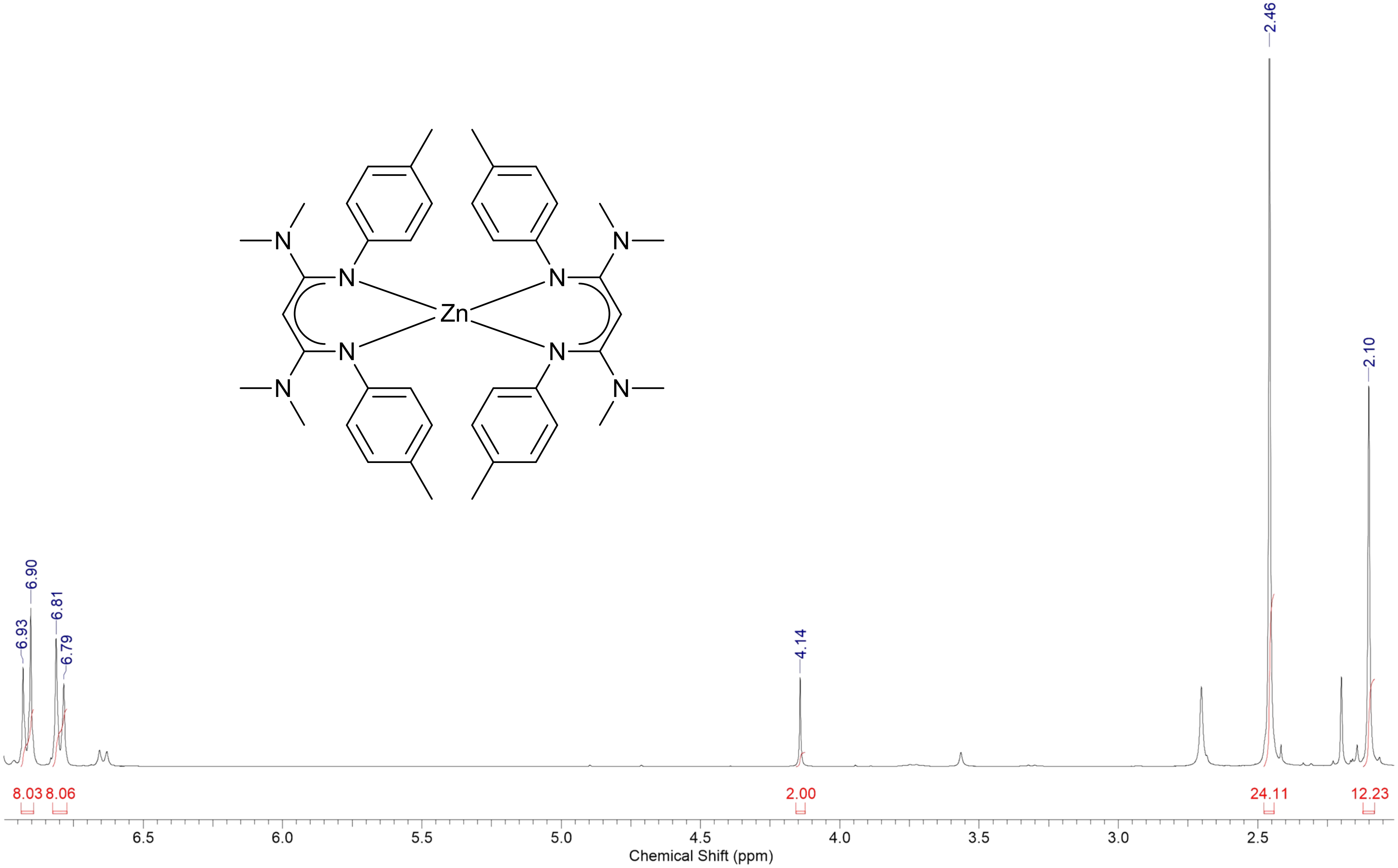

Figure S35: ^{1}H NMR spectrum of **16**, in C_6D_6. Residual **6** is present.

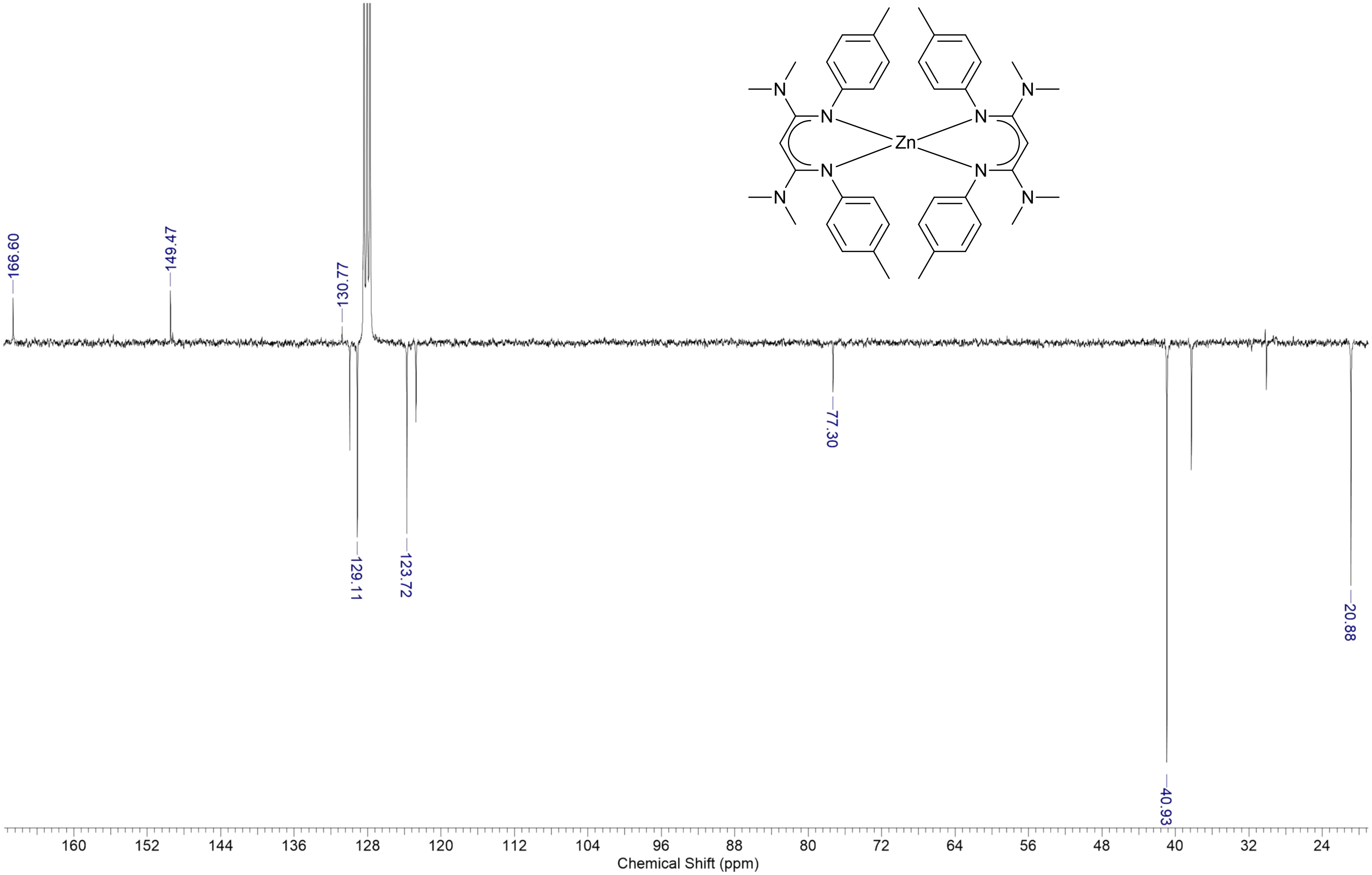

Figure S36: $^{13}C\{^1H\}$ DEPTQ NMR spectrum of **16**, in C_6D_6 (C_q & CH_2 ↑, CH & CH_3). Residual **6** is present.

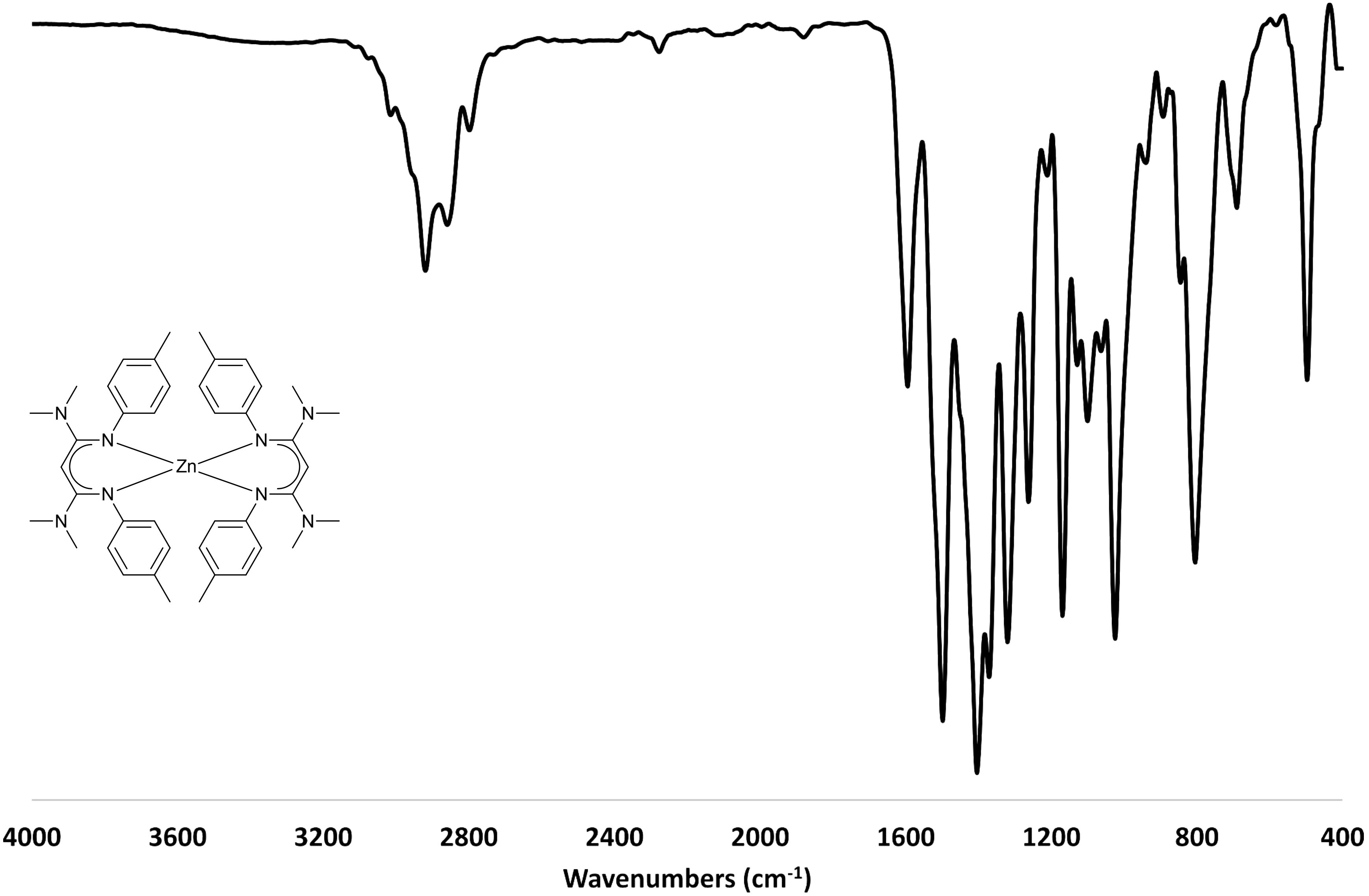

Figure S37: IR spectrum of **16**, obtained by ATR

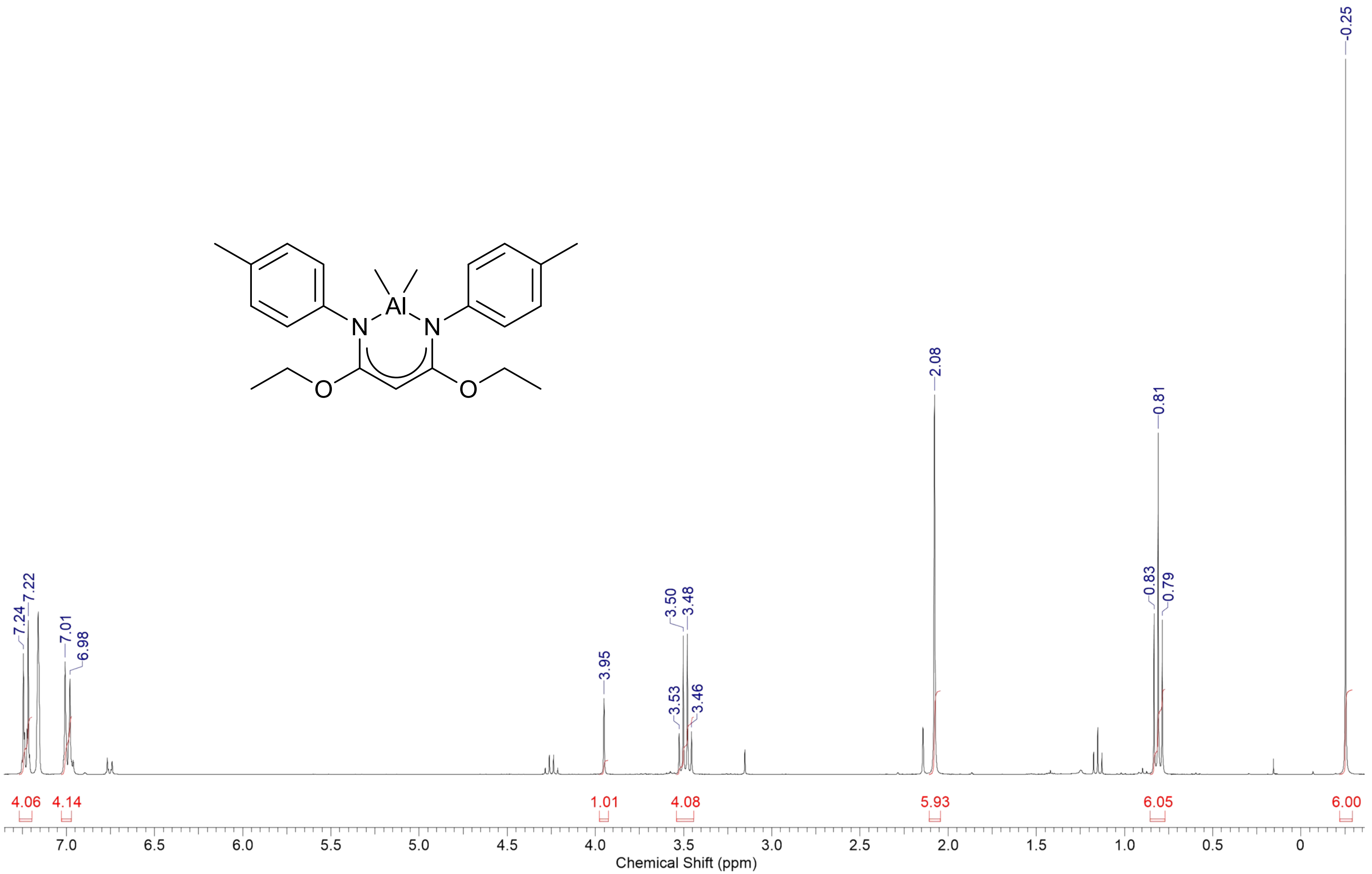

Figure S38: ^{1}H NMR spectrum of **17**, in C_6D_6.

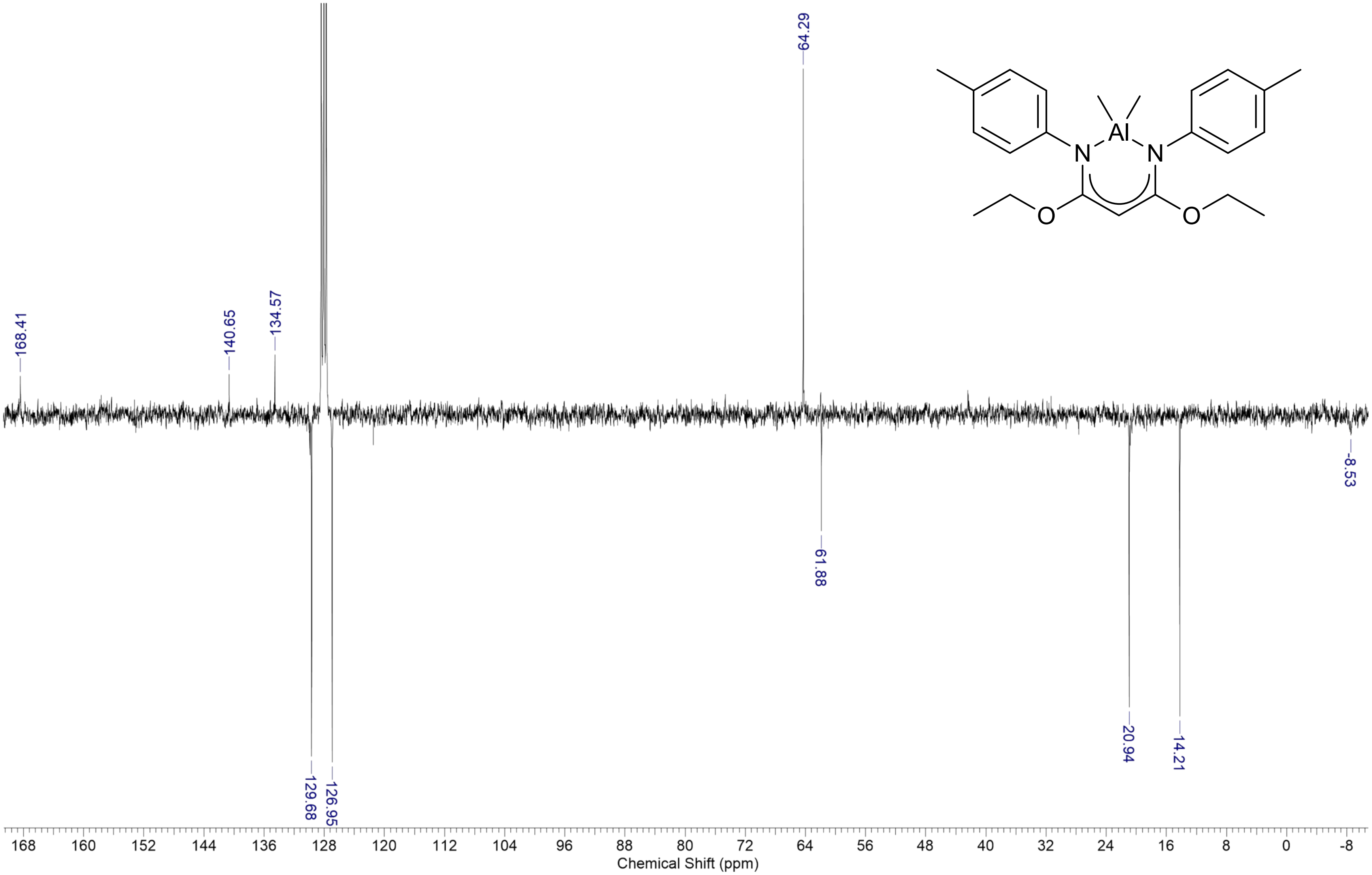

Figure S39: $^{13}C\{^{1}H\}$ DEPTQ NMR spectrum of **17**, in C_6D_6 (C_q & CH_2 ↑, CH & CH_3 ↓).

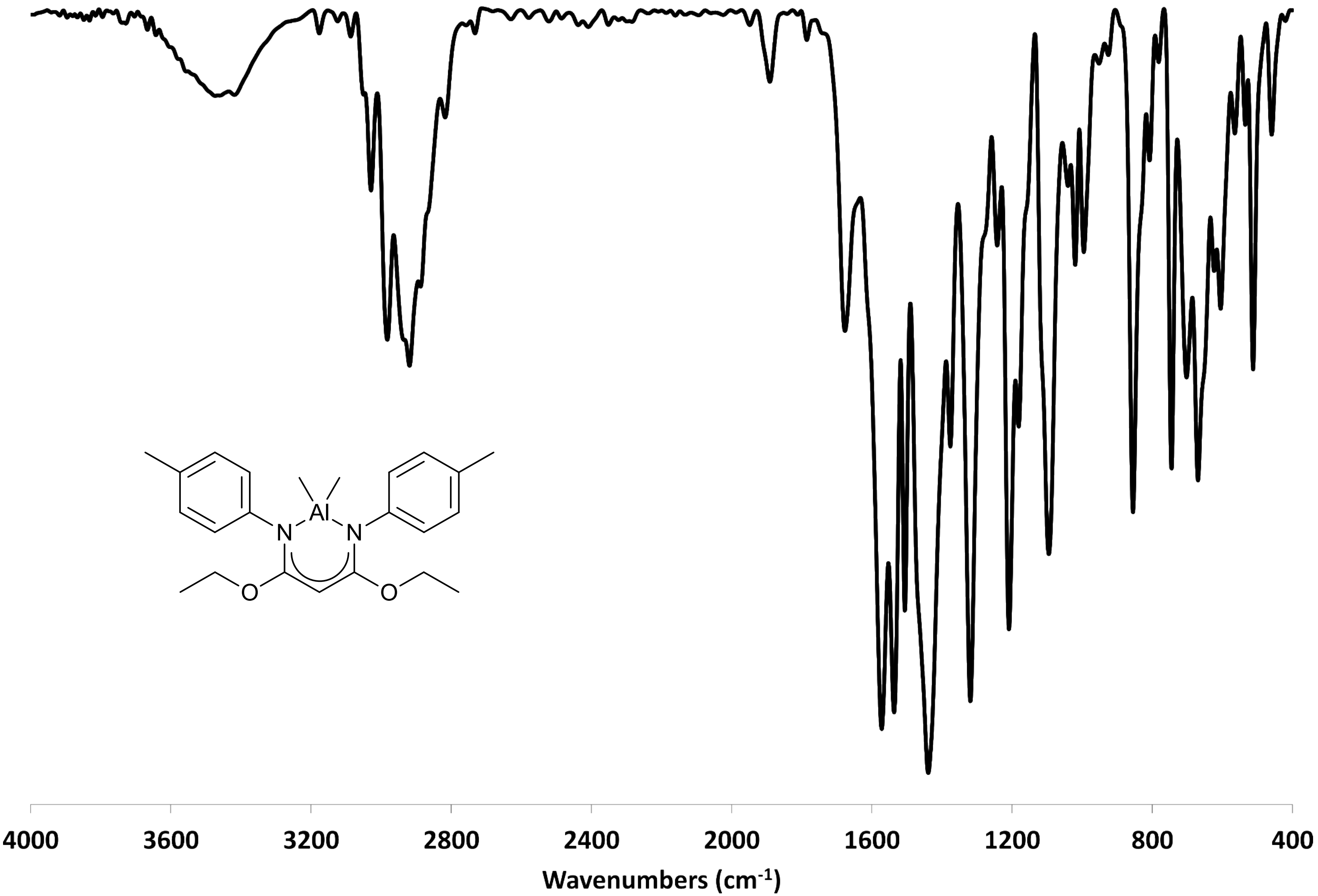

Figure S40: IR spectrum of **17**, obtained as a KBr pellet.

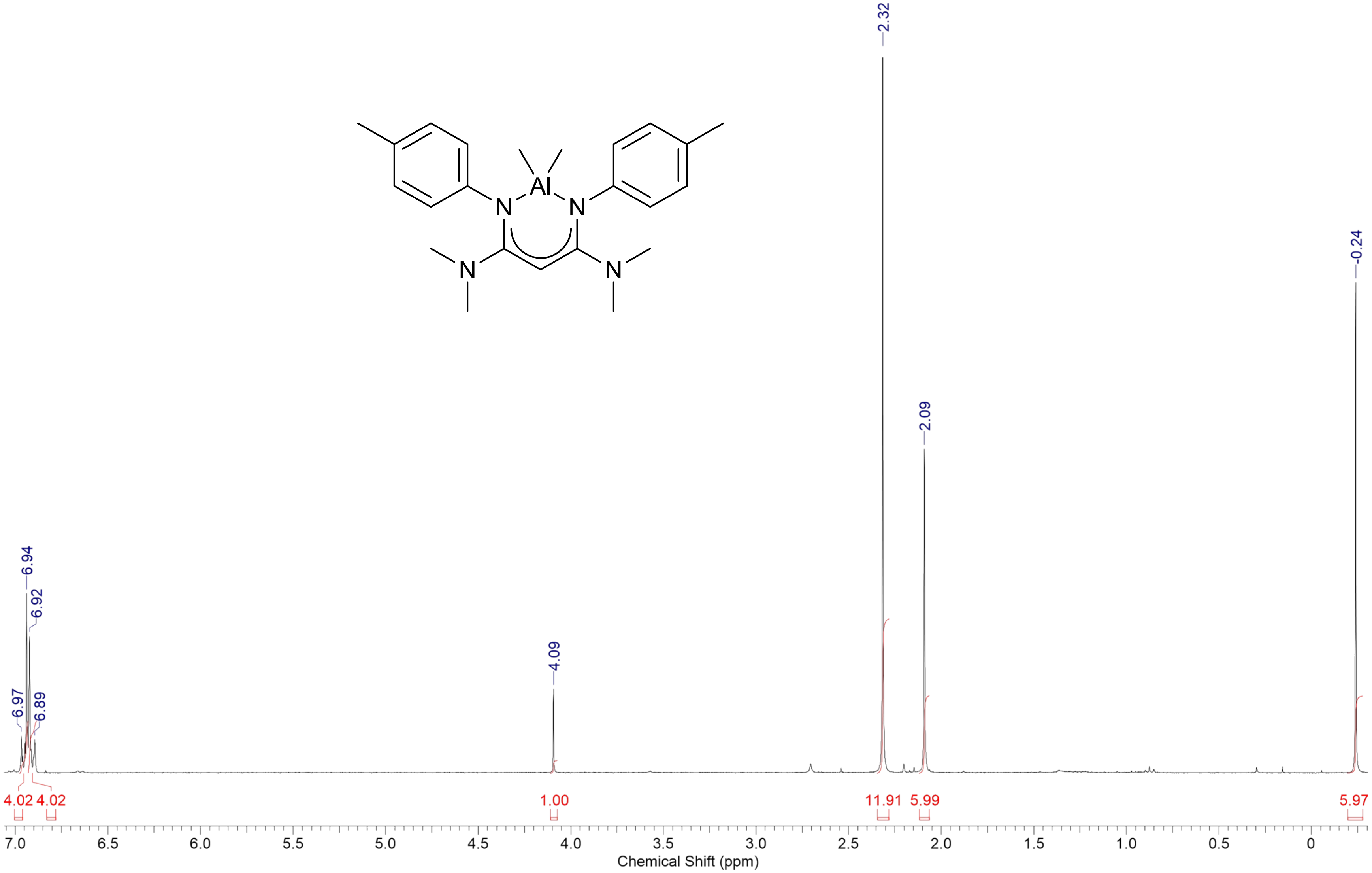

Figure S41: ^{1}H NMR spectrum of **18**, in C_6D_6.

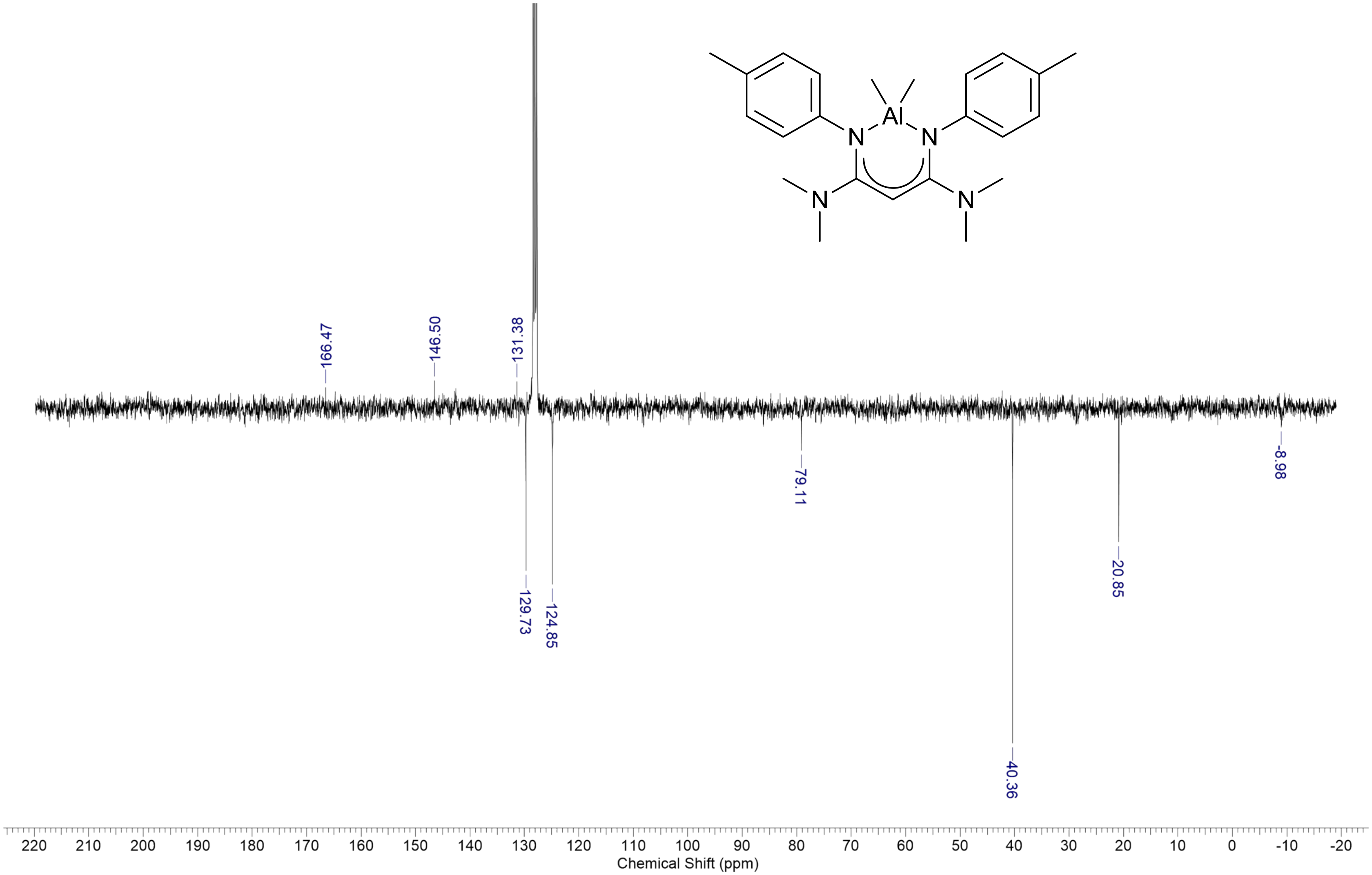

Figure S42: ^{13}C{^{1}H} DEPTQ NMR spectrum of **18**, in C_6D_6 (C_q & CH_2 ↑, CH & CH_3 ↓).

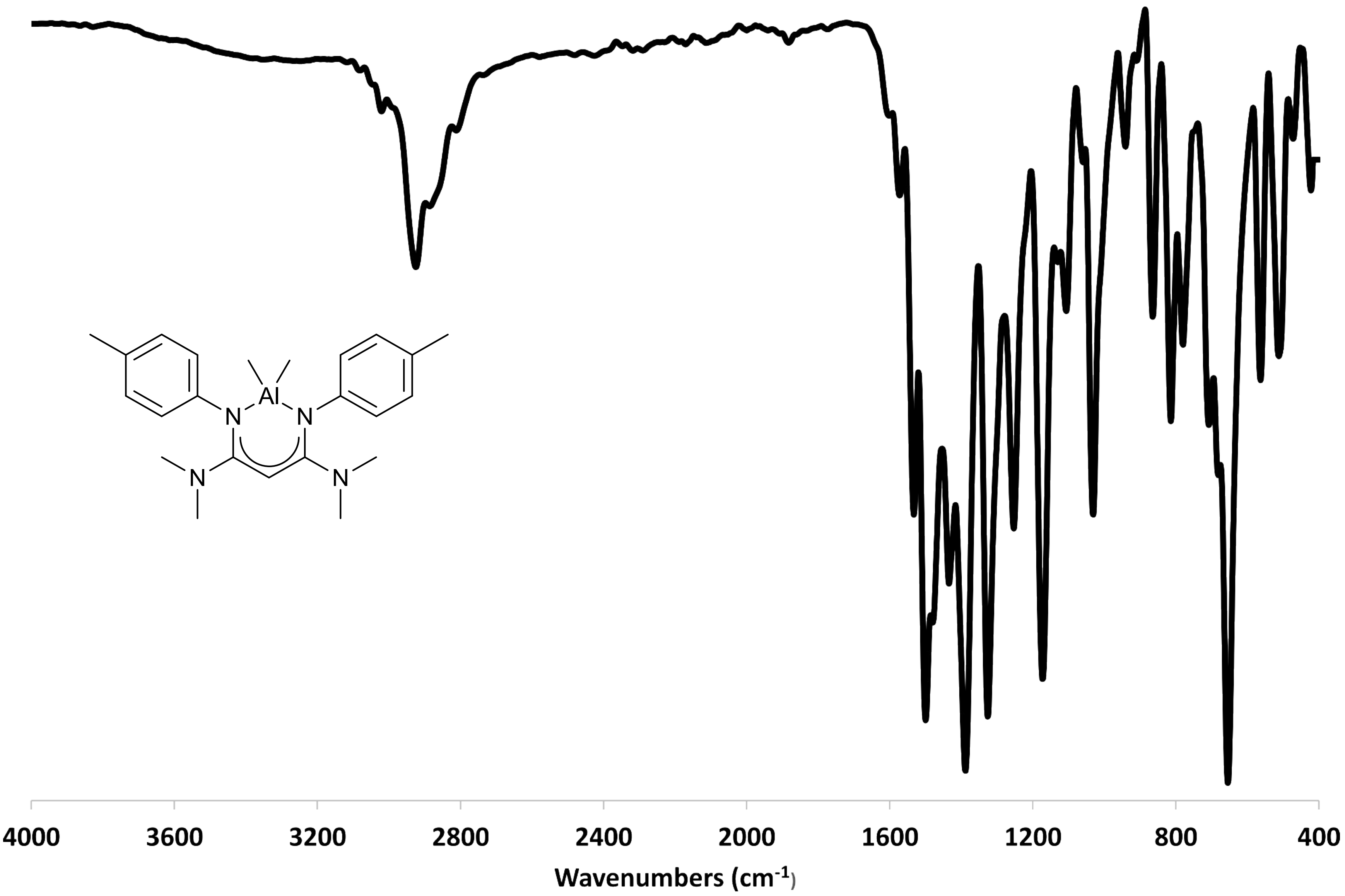

Figure S43: IR spectrum of **18**, obtain by ATR.